Contrib Mineral Petrol (2010) 160:683–704
DOI 10.1007/s00410-010-0502-6

ORIGINAL PAPER

Hydrous partial melting in the sheeted dike complex at fast spreading ridges: experimental and natural observations

Lydéric France · Juergen Koepke · Benoit Ildefonse · Sarah B. Cichy · Fabien Deschamps

Received: 6 August 2009 / Accepted: 10 February 2010 / Published online: 9 March 2010

Abstract In ophiolites and in present-day oceanic crust formed at fast spreading ridges, oceanic plagiogranites are commonly observed at, or close to the base of the sheeted dike complex. They can be produced either by differentiation of mafic melts, or by hydrous partial melting of the hydrothermally altered sheeted dikes. In addition, the hydrothermally altered base of the sheeted dike complex, which is often infiltrated by plagiogranitic veins, is usually recrystallized into granoblastic dikes that are commonly interpreted as a result of prograde granulitic metamorphism. To test the anatectic origin of oceanic plagiogranites, we performed melting experiments on a natural hydrothermally altered dike, under conditions that match those prevailing at the base of the sheeted dike complex. All generated melts are water saturated, transitional between tholeiitic and calc-alkaline, and match the compositions of oceanic plagiogranites observed close to the base of the sheeted dike complex. Newly crystallized clinopyroxene and plagioclase have compositions that are characteristic of the same minerals in granoblastic dikes. Published silicic melt compositions obtained in classical MORB fractionation experiments also broadly match the compositions of oceanic plagiogranites; however, the compositions of the coexisting experimental minerals significantly deviate from those of the granoblastic dikes. Our results demonstrate that hydrous partial melting is a likely common process in the root zone of the sheeted dike complex, starting at temperatures exceeding 850°C. The newly formed melt can either crystallize to form oceanic plagiogranites or may be recycled within the melt lens resulting in hybridized and contaminated MORB melts. It represents the main MORB crustal contamination process. The residue after the partial melting event is represented by the granoblastic dikes. Our results support a model with a dynamic melt lens that has the potential to trigger hydrous partial melting reactions in the previously hydrothermally altered sheeted dikes. A new thermometer using the Al content of clinopyroxene is also elaborated.

Keywords Mid-ocean ridge · Axial magma chamber · Hydrothermal system · Sheeted dike complex · Partial melting · Experimental petrology · Oceanic plagiogranite · Granoblastic dikes

Communicated by J. Hoefs.

Electronic supplementary material The online version of this article (doi:10.1007/s00410-010-0502-6) contains supplementary material, which is available to authorized users.

L. France · B. Ildefonse
Géosciences Montpellier, CNRS, Université Montpellier 2, CC60, 34095 Montpellier Cedex 05, France
e-mail: france@gm.univ-montp2.fr

L. France (✉) · J. Koepke · S. B. Cichy
Institut für Mineralogie, Leibniz Universität Hannover, Callinstrasse 3, 30167 Hannover, Germany

F. Deschamps
LGCA UMR CNRS 5025, Université Joseph-Fourier, BP 53, 38041 Grenoble cedex, France

Present Address:
L. France
Géosciences et Environnement Cergy, Université Cergy-Pontoise, 5 mail Gay Lussac, Neuville sur Oise, 95031 Cergy-Pontoise cedex, France
lyderic.france@u-cergy.fr

Introduction

At fast spreading ridges, the root zone of the sheeted dike complex is a peculiar geological horizon where the thermal

gradient can be as high as 7°C/m, one of the highest, continuously present gradient observed on earth (Nicolas et al. 2008). Moreover, the contact of the sheeted dike complex with the underlying melt lens can be regarded as an interface between two convecting systems, the magmatic and the hydrothermal one. Highly hydrothermally altered basaltic rocks from the base of the sheeted dike complex are therefore in the vicinity of a relatively constant heat source, which has the potential to trigger dehydration and/or melting reactions. Nicolas et al. (2008) have studied in the Oman ophiolite the varitextured gabbro horizon located directly below the sheeted dike complex and have interpreted most of the observed lithologies as hydrous partial melting products. Gillis and Coogan (2002), Wilson et al. (2006), Gillis (2008) and Koepke et al. (2008) investigated the base of the sheeted dike complex in the Troodos ophiolite, in the Oman ophiolite, and in IODP (Integrated Ocean Drilling Program) Hole 1256D. They describe typical granoblastic, hornfelsic lithologies in amphibolite- to granulite-facies and relate them to reheated, dehydrated sheeted dikes ("granoblastic dikes"). To further understand the active processes at the sheeted dike/gabbro transition, France et al. (2009a) have compared this zone in the Oman ophiolite with the recent IODP Hole 1256D and propose a dynamic model with up- and downward migrations of the gabbro/sheeted dike interface that is consistent with published models and descriptions of Gillis and Coogan (2002), Wilson et al. (2006), Gillis (2008) and Koepke et al. (2008). The mobility of the melt lens is supported by the observed reheating of the base of the sheeted dike complex and recycling of the previously hydrothermally altered sheeted dikes in the underlying varitextured gabbros. The occurrence of partly assimilated sheeted dikes fragments within the uppermost gabbros suggests that the lowermost sheeted dikes underwent hydrous partial melting.

Oceanic plagiogranites, as defined in Koepke et al. (2007), are common in the oceanic crust, in particular at the base of the sheeted dike complex (e.g., Pallister and Hopson 1981), where they are generally found as relatively small bodies (Koepke et al. 2004, 2007). These oceanic plagiogranites are believed to represent products of either differentiated MORB, or liquid immiscibility resulting in the occurrence of a mafic and of a felsic melt, or hydrous partial melting of gabbros or sheeted dikes. Formation from MORB differentiation has been proposed in natural settings (e.g., Beccaluva et al. 1977; Coleman and Donato 1979; Dubois 1983; Lippard et al. 1986; Amri et al. 1996; Floyd et al. 1998; Selbekk et al. 1998; Beccaluva et al. 1999; Niu et al. 2002; Rao et al. 2004; Bonev and Stampfli 2009; Rollinson 2009) and has also been verified in experimental studies (Dixon-Spulber and Rutherford 1983; Berndt et al. 2005; Feig et al. 2006). Liquid immiscibility has been observed in rapidly quenched basaltic flows from the upper oceanic crust (e.g., Sato 1978; Philpotts 1982), inferred from ophiolites (Ménot 1987; Ulrich and Borsien 1996; Shastry et al. 2001), and described experimentally (Dixon and Rutherford 1979; Veksler et al. 2007).

Natural occurrences and previous experiments on hydrous partial melting of mafic rocks

Hydrous partial melting of mafic rocks has been proposed or described in several studies (e.g., Malpas 1979; Gerlach et al. 1981; Pedersen and Malpas 1984; Flagler and Spray 1991; Spray and Dunning 1991; Twinning 1996; Floyd et al. 1998; Selbekk et al. 1998; Gillis and Coogan 2002; Coogan et al. 2003; Stakes and Taylor 2003; Koepke et al. 2004, 2005a; Luchitskaya et al. 2005; Koepke et al. 2007; Nicolas et al. 2008; Rollinson 2009). Most of these studies deal with ophiolites and attempt to determine the origin of plagiogranitic rocks. The interpretation of an anatectic origin is based on structural evidences and/or on trace element geochemical modeling. Evidence of hydrous partial melting of mafic lithologies has also been reported from young oceanic crust at both slow spreading (e.g., Mével 1988) and fast spreading (e.g., Koepke et al. 2005b, 2008) centers. The partial to complete assimilation of previously hydrothermally altered sheeted dikes, in magma chambers at fast spreading ridges, implies that the assimilated hydrothermally altered rocks undergo hydrous partial melting. This recycling process is described in ophiolites (Coogan et al. 2003; Gillis 2008; France et al. 2009a) and in present-day oceanic crust (Wilson et al. 2006; Koepke et al. 2008; France et al. 2009a), or inferred from chlorine contents in amphiboles (Coogan 2003; Coogan et al. 2003) and MORB (e.g., Michael and Schilling 1989).

Experimental work that precisely matches the conditions (low pressure, high temperature, hydrous and highly oxidizing conditions as highlighted by Koepke et al. (2008), Nicolas et al. (2008), and France et al. (2009a)) and the basaltic composition associated with a strong hydrothermal alteration prevailing at the base of the sheeted dike are lacking. Several experimental studies (e.g., Beard and Lofgren 1989; Hacker 1990; Beard and Lofgren 1991; Rapp et al. 1991; Rushmer 1991, 1993; Sen and Dunn 1994; Wolf and Wyllie 1994; Rapp and Watson 1995; Patino Douce and Beard, 1995; Prouteau et al. 1999; Johannes and Koepke, 2001) have focused on the melting of mafic lithologies to investigate the origin of Archean tonalites, trondhjemites, and granodiorites (TTG rocks; Barker 1979), which are believed to result from dehydration melting of amphibolites. Other authors have studied the melting of basalts in hydrous environment (Holloway and Burnham, 1972; Helz 1973; Beard and Lofgren, 1991;

Kawamoto, 1996). Although some of these works approach the appropriate natural conditions (e.g., Beard and Lofgren, 1991), they are not fully relevant to the study of hydrous melting at the base of the sheeted dikes. These studies deal with subduction processes, and most of them are conducted at pressures (in general ≥500 MPa) that are much higher than those (~100 MPa) prevailing at the base of the upper, basaltic oceanic crust. Moreover, most of these studies use dehydration melting experiments which are valid for the subduction environment but not for the base of the sheeted dikes where a lot of water is available at low pressure, resulting in water-saturated conditions. The study of Beard and Lofgren (1991) approaches those conditions relevant to partial melting/assimilation of hydrothermally altered sheeted dikes at the gabbro/dike transition. Unfortunately, they do not provide the mineral compositions, and the redox conditions are not fixed but roughly estimated. The redox conditions, which are influenced by the presence of a high temperature hydrothermal system at the base of the sheeted dike complex (Nicolas et al. 2008), must be precisely controlled to understand and follow the evolution of melt and minerals with temperature. Koepke et al. (2004) have performed hydrous partial melting experiments on gabbroic lithologies from the lower oceanic crust with controlled redox conditions, but these experiments are not applicable to hydrous partial melting at the base of the sheeted dike complex. Hydrous partial melting of sheeted dike complex and gabbros may produce different melts and different residual phases because of different composition and mineralogy of the used starting material. While typical oceanic gabbros show a marked refractory character (e.g., extremely depleted in incompatible elements like Ti and K; mostly high in Mg#, with Mg# = Mg/[Mg + Fe]), most sheeted dikes are more fractionated with compositions of evolved MORB (e.g., Pallister and Knight, 1981; Ross and Elthon, 1993; Wilson et al. 2006). Another characteristic feature of the dikes at the gabbro/dike transition is related to significant hydrothermal alteration responsible for the formation of considerable amounts of hydrous minerals, which affects the melting behavior of a rock, in particular at lower temperatures, where the completion of a global equilibrium is often hampered.

Experimental and analytical techniques

Starting material

In order to closely match natural processes, we have selected a representative sample (08OL30) of typically hydrothermally altered sheeted dikes from the Oman ophiolite. It has been sampled in the Aswad area located in the southern Sumail massif, which is inferred to correspond to typical

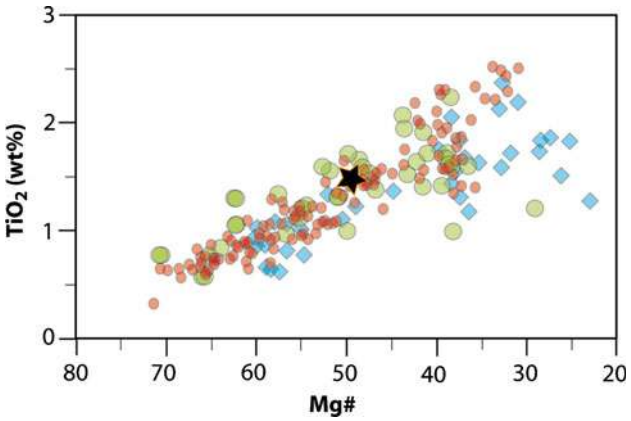

Fig. 1 Comparison of the bulk rock composition of the starting material (08OL30) with those of sheeted dike complex and extrusives of the Oman ophiolite in a TiO_2 versus Mg# diagram (with Mg# = Mg/[Mg + Fe_{total}]); after Miyashita et al. (2003). *Symbols* are *black star*: starting material, *red small circle*: sheeted dike complex by Miyashita et al. (2003), *green large circle*: sheeted dike complex by Lippard et al. (1986), and Type 1 dikes by Rochette et al. (1991), *blue diamonds*: Geotimes volcanics by Lippard et al. (1986) and V1 lava by Einaudi et al. (2000)

oceanic crust away from ridge discontinuities, and not affected by ridge tectonics or obduction-related deformation (Nicolas et al. 2000; Nicolas et al. 2008). Its whole-rock composition is representative of typical sheeted dikes from the Oman ophiolite (Fig. 1; Table 1). Compared to the average sheeted dike rocks sampled at ODP/IODP Hole 1256D and ODP Hole 504B, at Hess Deep, and at the Blanco Depression (Table 1), the chosen starting material is slightly more evolved. It is strongly altered due to a static hydrothermal overprint, which is a common feature of the sheeted dike complex in the studied area. The selected sample is composed of albitized plagioclase (An_{03}), actinolite, prehnite, pumpellyite, titanite, and some magnetite (Fig. 2), an assemblage typical of greenschist-facies conditions (see section "Phase compositions in the partial molten system" for mineral compositions; Table 1, electronic supplementary item). Primary magmatic phases are not observed.

After crushing the starting rock, three grain size fractions were obtained by sieving (30–100, 100–150, and 150–250 μm) and were used for preliminary experiments. These experiments were performed at a temperature of 1,000°C to study the effect of grain size of the starting material on the kinetics of the melting reaction (Table 2). In the three experimental products, minerals and melts have identical compositions within the analytical errors (Table 2, electronic supplementary item). Moreover, the phases are homogeneous, crystals display no zonation, and compositions are identical within the whole capsule volume, independent of the grain size of the starting material (Fig. 3a). No relict phases of the starting material were observed. As experiments performed with coarser grain

Table 1 Whole-rock compositions of the starting material and of sheeted dike complex from different oceanic localities

	SiO_2	TiO_2	Al_2O_3	Fe_2O_3(t)	MnO	MgO	CaO	Na_2O	K_2O	P_2O_5	LOI	Total	Mg#
080L30	50.38	1.40	15.04	10.29	0.06	4.99	7.19	4.44	0.19	0.11	4.74	98.82	–
080L30_recalculated	53.55	1.48	15.98	10.94	0.07	5.30	7.64	4.72	0.20	0.12	–	100.00	49.0
Oman, Umino et al. 2003	52.51 ± 2.09	1.17 ± 0.45	16.06 ± 0.92	10.41 ± 1.83	0.15 ± 0.05	6.68 ± 1.28	8.51 ± 2.81	4.21 ± 1.34	0.18 ± 0.15	0.11 ± 0.03	–	100.00	56.0
Oman, Miyashita et al. (2003)	52.59 ± 1.72	1.33 ± 0.50	15.64 ± 0.76	10.89 ± 2.16	0.16 ± 0.05	6.03 ± 1.55	8.86 ± 2.68	4.24 ± 1.39	0.16 ± 0.12	0.11 ± 0.05	–	100.00	52.3
1256D, Teagle et al. (2006)	50.56	1.55	13.75	13.57	0.23	6.88	10.75	2.53	0.05	0.13	–	100.00	50.1
Hess Deep, Pollock et al. (2009)	50.57	1.37	14.31	11.58	0.20	8.02	10.82	2.78	0.05	0.31	–	100.00	57.8
504B, Bach et al. (1996)	49.36	0.80	16.12	9.60	0.15	8.93	13.11	1.86	0.01	0.06	–	100.00	64.8
Blanco Depression, Cordier et al. (2007), Juteau et al. (1995)	50.08	1.99	13.97	13.15	0.21	6.79	10.60	2.82	0.22	0.16	–	100.00	50.5

Composition of the sheeted dike complex from Oman (Umino et al. 2003; Miyashita et al. 2003), from IODP Hole 1256D in the Cocos plate (Teagle et al. 2006), from Hess Deep (East Pacific Rise [EPR]; Pollock et al. 2009), from ODP Hole 504B (Bach et al. 1996), and from the Blanco Fracture Zone on the Juan de Fuca ridge (average of data from Juteau et al. 1995 and Cordier et al. 2007). For comparison, compositions of sample 080L30 (starting material) are recalculated at 100%. Standard deviations are given for the Oman sheeted dike. Mg# = Mg/(Mg + Fe_{total}); *LOI* loss on ignition

size produce larger experimental crystals and melt pools (e.g., Koepke et al. 2004), which are more suitable for electron microprobe measurements, we chose the 150- to 250-μm fraction as starting material.

Experimental method

Melting experiments (≥850°C) have been performed in an internally heated pressure vessel (IHPV) at the experimental laboratory of the Institut für Mineralogie (Hannover, Germany), equipped with a Shaw membrane and a rapid quench device. Details of the IHPV are presented in Berndt et al. (2002). The vessel was pressurized with argon at 100 MPa, a pressure relevant to the level of the axial melt lens within the ocean crust. The pressure was controlled with a strain gauge manometer (uncertainty of ±5 MPa). Previous calibrations on the vessel show that temperature is homogeneous over the sample with less than 10°C of variation and a measurement accuracy better than ±10°C. This is also indicated by the regular evolution of the melt and mineral compositions with temperature (see section "Phase compositions in the partial molten system"). Experimental conditions are summarized in Table 2. In all experiments, the prevailing fO_2 corresponds to FMQ+1–FMQ+2 (FMQ relation after Ballhaus et al. 1991), where FMQ is the fayalite–magnetite–quartz oxygen buffer equilibrium (for values see Table 2). At the beginning of the experiment, the temperature rises continuously (30°C/min) to reach the final experimental temperature after ~30 min. At the end of experiment, the samples were quenched isobarically using a rapid quench facility to prevent crystallization during cooling (~150°C/s). Effective quenching is evidenced by the absence of "quench minerals" in melts in spite of the presence of low viscosity basaltic melts with high water content.

In addition to the high temperature runs in the partially molten regime, subsolidus experiments (750°C and 800°C) have been performed in an externally heated cold-seal pressure vessel (CSPV). This vessel was pressurized with water at 100 MPa and controlled with a pressure transducer calibrated against a strain gauge manometer. The accuracy of pressure measurements was 1 MPa, and pressure variations during the experiments were less than ±5 MPa. The temperature was controlled with an external Ni–CrNi thermocouple (vessels were calibrated for temperature). The temperature variations were less than 5°C, while the accuracy was estimated to be ±10°C. Experimental conditions are summarized in Table 2. In all experimental runs, fO_2 corresponds to the NNO oxygen buffer (≈FMQ+1), established by adding a solid buffer composed of a Ni–NiO assemblage around the gold capsule. However, Scaillet et al. (1992) have shown that the maximum buffer lifetime is in the order of a few days, which is much less than the time spanned by our experiments. The

Table 2 Experimental conditions

RUN N°	Capsule	Temperature (°C)	f (H_2)	Δ_{FMQ}	Phases	Duration (h)	Grain size (μm)
#3	#10[D] #12[W]	1,030	2.18	1.38	melt, Ol, Cpx	72	150–250
#1	#2c[W]	1,000	2.77	1.56	melt, Ol, Cpx, Pl, TiMagt, Pl_m	72	150–250
	#3b[W]						100–150
	#4a[W]						30–100
#4	#13[D] #14[W]	970	1.89	1.51	melt, Ol, Cpx, Pl, TiMagt, Pl_m	96	150–250
#7	#23 [D] #25[W]	955	2.63	1.24	melt, Ol, Cpx, Pl, TiMagt, Ilm, Pl_m	96	150–250
#6	#17[D] #18[W]	940	2.02	1.45	melt, Ol, Cpx, Pl, Amp, Opx, TiMagt, Ilm, Pl_m, Titanite, Apatite	96	150–250
#2	#5[D] #8[W]	910	2.24	1.36	melt, Cpx, Pl, Amp, Opx, TiMagt, Ilm, Pl_m, Titanite	120	150–250
#5	#15[D] #16[W]	880	0.97	2.09	melt, Cpx, Pl, Amp, Opx, TiMagt, Ilm, Pl_m, Titanite, Act	120	150–250
#8	#24[D] #26[W]	850	2.53	1.13	Melt, Cpx, Pl, Amp, Opx, TiMagt, Ilm, Pl_m, Titanite, Act	144	150–250
#metam 1	#9[D] #11[W]	800	–	NNO	Pl, Amp, Opx, TiMagt, Ilm, Titanite, Act, Ab (+Pl_m + Cpx)	504	150–250
#metam 2	#21[D] #22[W]	750	–	NNO	Pl, Amp, Opx, TiMagt, Ilm, Titanite, Act, Ab (+Pl_m + Cpx)	624	150–250

D experiment without water addition, *W* experiment with water addition. The oxygen fugacity is given in log units relative to the FMQ oxygen buffer. Minerals in parentheses (+Pl_m + Cpx) are localized in the prehnite reaction zones (see "Prehnite breakdown reaction" part for further details). *Ol* olivine, *Cpx* clinopyroxene, *Pl* plagioclase, *TiMagt* titanomagnetite, Pl_m metastable plagioclase, *Ilm* ilmenite, *Amp* amphibole, *Opx* orthopyroxene, *Act* actinolite, *Ab* albite, *Magt* magnetite

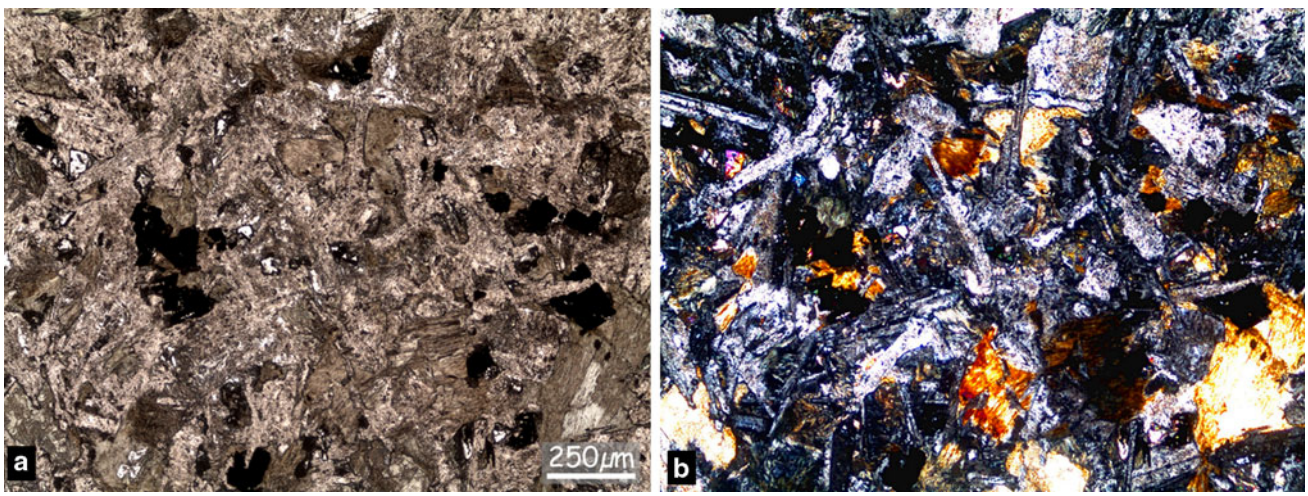

Fig. 2 Microphotographs of the starting material (08OL30). **a** plane-polarized light, **b** cross-polarized light

redox conditions are nevertheless considered to be close to the NNO buffer because of the vessel composition (Ni) and of the use of water for pressurization (Klimm et al. 2003). After experiments, samples were quenched isobarically by using a flux of compressed air (initial cooling rate ~200°C/min). For all the experiments, gold was used as capsule material. Thus, iron diffusion into the capsule material can be neglected.

Since the natural samples from the root zone of the sheeted dike complex contain high amounts of hydroxyl-

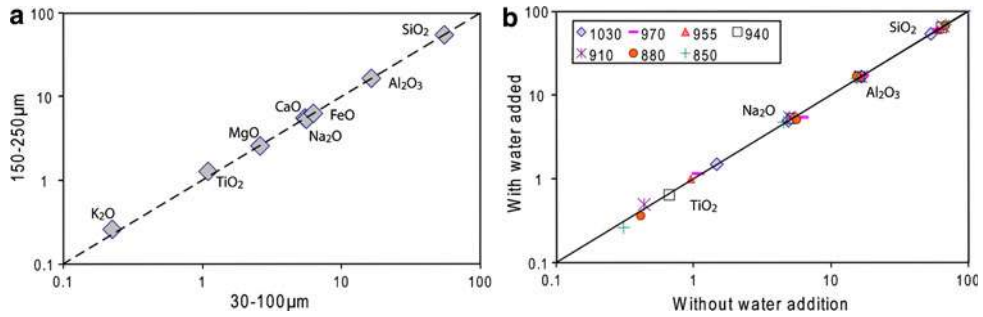

Fig. 3 Comparison of melt compositions from experiments performed with identical starting compositions (wt%) for different grain sizes of the starting material (**a**). Each data point represents the average for one oxide (as indicated). The corresponding experiments were performed at 1,000°C. **b** Comparison of melt compositions from experiments performed with identical starting compositions (wt%) for experiments with and without water added shown for the TiO_2, Na_2O, Al_2O_3, and SiO_2 at different temperatures. In both logarithmic plots, the line represents the 1:1 correlation. Grain size (**a**) and the addition of water to the starting material (**b**) have no influence on the melt composition

bearing minerals (actinolite, prehnite, pumpellyite), it was expected that water would be released in the partial melting experiments (dehydration melting). Due to the relatively low water solubility in basaltic melts at the given shallow pressure of 100 MPa (~3% according Hamilton et al. 1964, and ~3.3% according Berndt et al. 2002), water saturation in the experiments was expected. We performed one experimental series under water-saturated conditions by adding distilled water (5 mg) to the starting material (50 mg) and another series without adding water, corresponding to typical dehydration experiments. The two capsules (with and without water addition) were run simultaneously at each temperature. For each temperature, results from both capsules are identical for the phase relations and phase compositions (Fig. 3b; melt and phase compositions of experiments with and without water additions are presented Table 2, electronic supplementary item), suggesting that in both experimental series, water saturation was reached and that the dehydration melting produces enough water for reaching water-saturated condition. In all experiments, bubbles are present, attesting fluid (mainly composed of water) saturation (Fig. 4). The similarity between the two series shows that experiments are reproducible, in order to clarify figures; an average value of both series will be used all along the results presentation and discussion.

Analytical method

Experimental samples were analyzed using a Cameca SX100 electron microprobe (Institut für Mineralogie, Hannover, Germany) equipped with 5 spectrometers, "Peak sight" software is used. All analyses were performed using a 15 kV acceleration potential, a static (fixed) beam, Kα emission from all elements. The matrix correction is based on Pouchou and Pichoir (1991). Analyses of crystals were performed with a beam current of 15 nA using a focused beam and a counting time of 10 to 30 s on peak and background. Analyses of glasses were performed with a beam current, which was set to 6 nA to minimize migration and volatilization of the alkali elements. Counting time was from 2 to 5 s for Na and K and from 5 to 10 for other elements (Si, Ti, Al, Mg, Fe, Ca, Mn, Cr). In the experiments where melt pools are large enough, the beam was defocused to a spot size of 5 to 20 µm. To test the suitability of glass analyses performed with focused beam (when melt pools are too small), some large melt pools were analyzed with focused and defocused beams; both results were homogeneous. Backscattered electron (BSE) images were also obtained on the Cameca SX100 electron microprobe.

Experimental results

Attainment of equilibrium

The use of fine-grained starting material (≤10 µm) in partial melting experiments enhances the achievement of global equilibrium. Unfortunately, it prevents suitable microprobe analyses due to very small newly formed experimental phases. The advantage of using coarser grained starting material is the formation of relatively large crystals in the experimental products, which enables easy

Fig. 4 Backscattered electron images of the experimental results in the partly molten system for different temperatures **a** 1,030°C with water added (melt proportion is not representative for the whole sample which shows >90% melt); **b** 1,000°C with water added; **c** 970°C with water added; **d** 940°C without water addition; **e** 910°C without water addition; **f** 880°C without water addition; **g** numerous tiny oxide inclusions in clinopyroxene and olivine in the experiment performed at 970°C without water addition; **h** "metastable plagioclase" in the experiment performed at 1,000°C with water added. Minerals abbreviations are the same as in Table 2 ▶

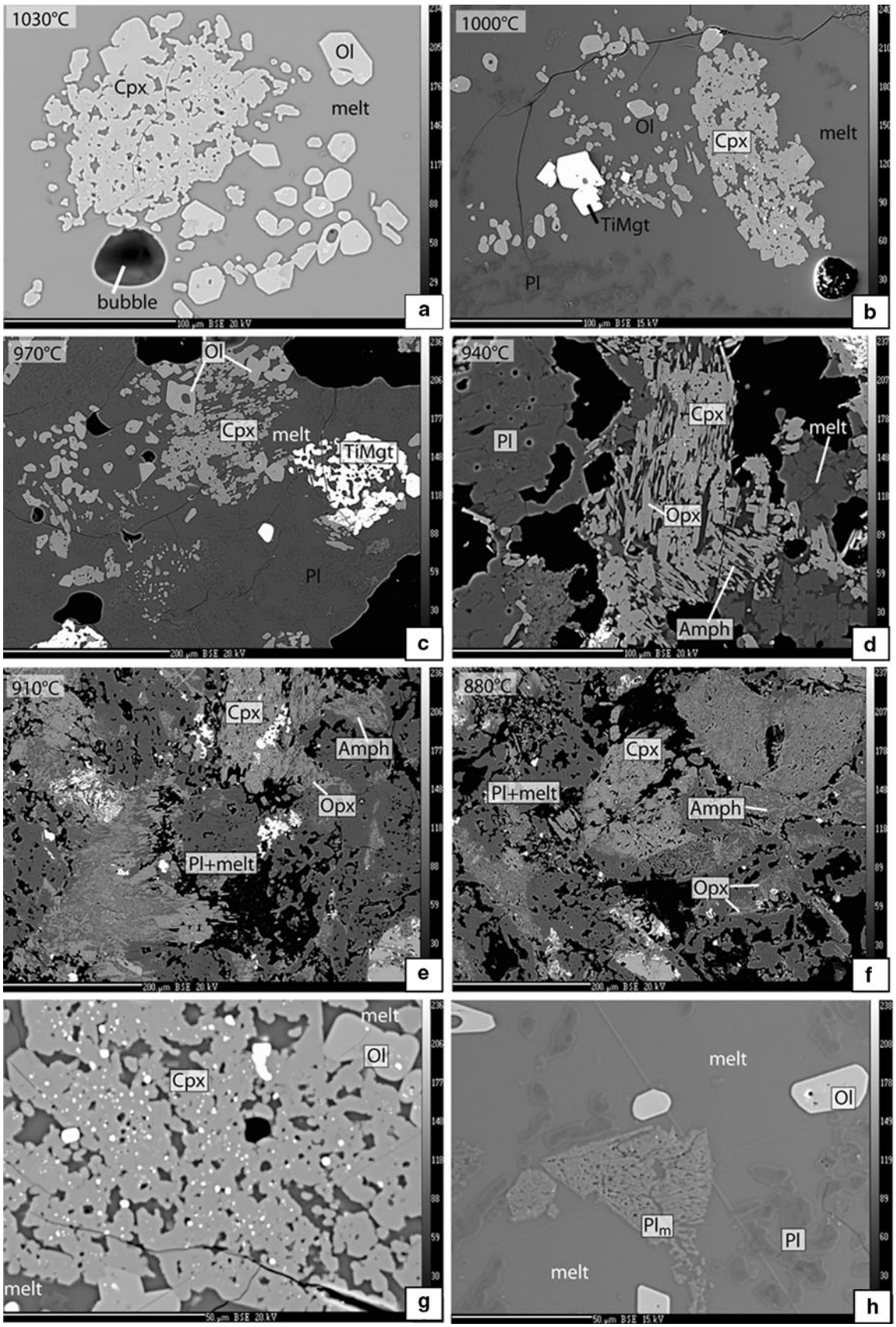
1030°C
Ol
Cpx
melt
bubble
a
1000°C
Ol
Cpx
melt
TiMgt
Pl
b
970°C
Ol
Cpx
melt
TiMgt
Pl
c
940°C
Cpx
melt
Pl
Opx
Amph
d
910°C
Cpx
Amph
Opx
Pl+melt
e
880°C
Cpx
Pl+melt
Amph
Opx
f
melt
Ol
Cpx
melt
g
melt
Ol
Pl_m
Pl
melt
h

microprobe analyses of the experimental phases. However, too coarse-grained starting material may prevent the achievement of global equilibrium, since cores of unreacted starting material may be still present after the experiment, as observed in many typical dehydration melting experiments of mafic protoliths (e.g., Hacker, 1990; Beard and Lofgren, 1991; Patino Douce and Beard 1995; Johannes and Koepke 2001). This effect is most pronounced concerning plagioclase, which is the rate-controlling phase in many basaltic systems (Johannes and Koepke 2001). These authors show that reaction kinetics can be significantly enhanced in water-saturated systems, as it was the case in our experiments. Moreover, the starting material in our experiments shows a pervasive alteration overprint (plagioclase with An < 03, actinolite, titanite, prehnite, pumpellyite, magnetite), and no typical primary magmatic phases (e.g., olivine, pyroxene, An-rich plagioclase, or magmatic amphibole) were present. Hence, the phase assemblage had to change completely during the melting reaction, thus minimizing the risk of formation of typical core/rim complexes of the reacting minerals. Moreover, tracking residual phases in experimental products will be facilitated. Due to the favorable conditions in our melting experiments, no relics of the starting material are present in most of the melting experiments, in particular those experiments performed at temperatures >910°C; an approach of the global equilibrium can therefore be proposed.

Several lines of evidence are listed below, which suggest that a state close to equilibrium has been attained in our "magmatic" experiments (i.e., temperatures >910°C): (1) No zonations in newly formed crystals are observed (Fig. 4), and crystal compositions are homogeneous within each experiment and between the two series (with and without addition of water). (2) Newly formed crystals (e.g., Ol) are commonly euhedral; when not (e.g., Cpx, Pl) large sponge-like grains mimic the shape of previous minerals. These sponge-like grains are homogenous in composition and widely infiltrated by melts, making easier the equilibrium approach (e.g., Fig. 4b–d). (3) No relictic phases from the starting materials are observed (for temperature >910°C). (4) All phase compositions vary systematically with temperature, and compositional trends are consistent with the ones expected from literature (e.g., rise of the plagioclase An content; see "Phase compositions in the partial molten system" section). (5) Glass compositions also vary systematically with temperature (see "Phase compositions in the partial molten system" section) and are homogeneous within each experiment and between the two series (with and without addition of water).

Nevertheless, a second type of plagioclase was sparsely observed in all experiments at temperatures ≤1,000°C. Compared to the equilibrium plagioclase which shows an idiomorphic habit, these are spongy with very irregular grain boundaries (Fig. 4h) and highly enriched in An component (Table 1, electronic supplementary item). These crystals are interpreted to represent metastable phases which were recrystallized after prehnite (for further details see section "Prehnite breakdown reaction"). Since these crystals occur only very rarely (largely less than 1% of the experimental result), we consider that the approaching of global equilibrium in these experiments is not hampered.

In subsolidus experiments, reactions are not complete, and new phases are only observed as coronitic assemblages. Therefore, these experiments will only be used to understand the metastable assemblages present in the partly molten system (see section "Prehnite breakdown reaction").

Phase relations in the partial molten system

The evolution of the phase relations (Fig. 5a) was established with the help of backscattered electron images (BSE; e.g., Fig. 4). Figure 5b gives a rough estimate of the phase proportions which were obtained via least square calculations (Albarède and Provost 1977). The first melt was observed at temperatures as low as 850°C, and the liquidus temperature is slightly higher than 1,030°C. While in the low-temperature experiment performed at 850°C melt pools seem to remain isolated, at temperatures >910°C the melt phase forms a connected framework. Melt proportion is low (<10%) for temperatures <910°C, and a large increase is observed between 940 and 970°C (Fig. 4); above 970°C, the melt proportion continues to increase linearly until the liquidus is reached. The liquidus phases are olivine and clinopyroxene; plagioclase and titanomagnetite are present below 1,000°C. The saturation of olivine and clinopyroxene at near-liquidus condition in tholeiitic systems is somewhat uncommon but can be ascribed to the high water activities as experiments are water saturated (e.g., Gaetani et al. 1993; Feig et al. 2006). First olivine appears at 940°C. Amphibole is stable in experiments up to 940°C. At this temperature, when applying the TiO_2 contents of amphibole to the semi-quantitative TiO_2-in-amphibole thermometer of Ernst and Liu (1998), the estimated temperature is 950°C and matches very well the run temperature, implying the achievement of equilibrium condition. The application of this thermometer is justified, since the amphibole in our experiments is coexisting with a Ti-rich oxide phase (Ernst and Liu 1998).

Orthopyroxene is stable up to 940°C. Application of the 2-pyroxene thermometer (Andersen et al. 1993) reveals equilibrium temperatures which are largely overestimated: 1,092 ± 31°C for the 940°C run; 1,039 ± 30°C for the 910°C run; 1,041 ± 36°C for the 880°C run, and

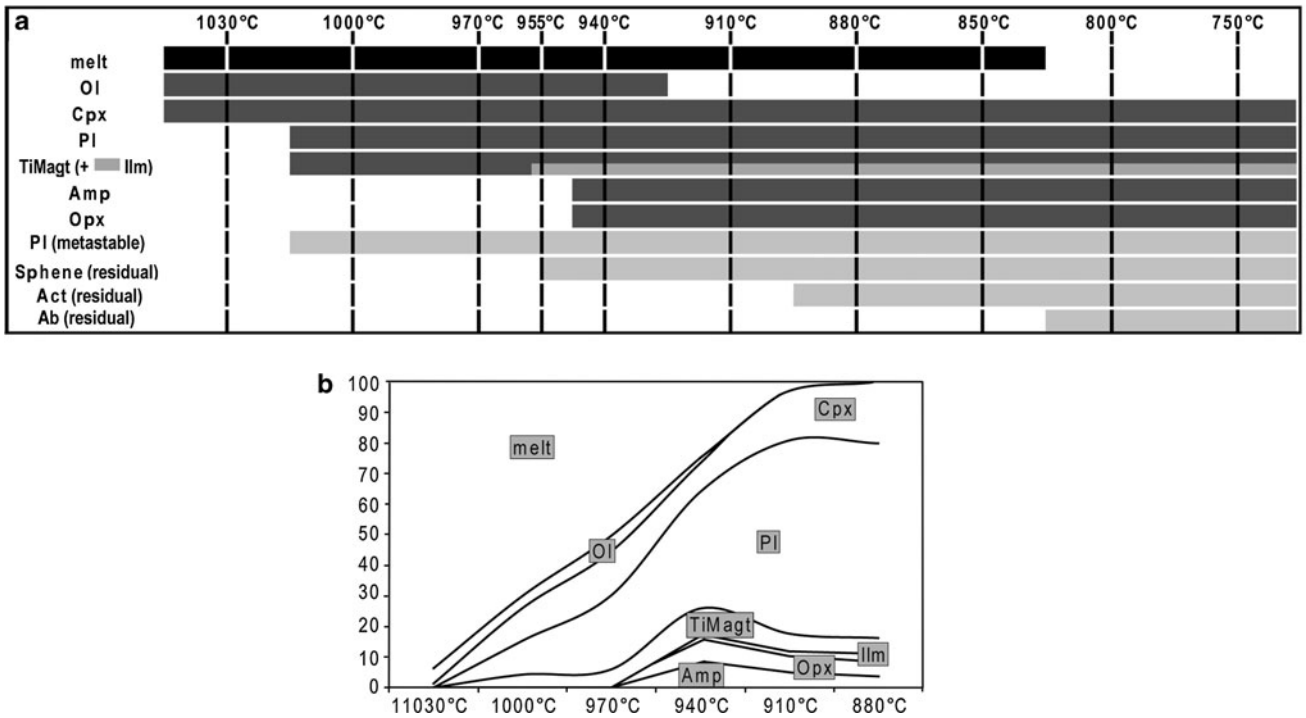

Fig. 5 **a** Phases present in the products of partial melting and subsolidus experiments as a function of temperature. Minerals abbreviations are the same as in Table 2. **b** Phase proportions in the partly molten system were calculated with a least square model according to Albarède and Provost (1977). Standard deviation <1 for all values. Values obtained for experiments at temperatures <950°C are less accurate. Incoherent values are obtained at 850°C. Minerals abbreviations are the same as in Table 2

1,056 ± 14°C for the 850°C run (data of Table 1, electronic supplementary item are used, these are averages of experiments with and without water addition). This large discrepancy can be explained by the presence of a high water activity, as the presence of water shifts the Mg# of clinopyroxene and orthopyroxene to higher values and consequently to higher calculated temperatures (Feig et al. 2006). Ilmenite is present up to temperatures of 955°C; at higher temperatures, only titanomagnetite is stable. Temperature and redox estimations calculated with the 2-oxide thermo-oxybarometer (Sauerzapf et al. 2008) are summarized in Table 3 (data of Table 1, electronic supplementary item are used for calculations, these are averages of experiments with and without water addition). The accuracy of the 2-oxide thermo-oxybarometer is ±70° for the temperature and ±0.4 log units for the oxygen fugacity (Sauerzapf et al. 2008). Hence, these estimations are consistent with the conditions of the experiments (Table 2). The new oxybarometer based on the total iron content present in clinopyroxene and in plagioclase (France et al. 2010) cannot be used here as it is restricted to melts with less than 60% of SiO_2. Numerous tiny oxides with grain sizes <5 μm were observed as inclusions in nearly all olivine and clinopyroxene grains (Fig. 4g). This observation is of significance, since similar features are observed in clinopyroxenes from the granulite-facies granoblastic dikes in natural settings (e.g., Koepke et al. 2008; France et al. 2009a), providing a tool for identifying such clinopyroxenes as residual phases after hydrous partial melting. Titanite is stable from low-temperature experiments to 940°C. In experiments from 910 to 1,000°C, some rare grains (largely less than 1% of the experimental result) of a metastable plagioclase (Pl_m) are observed (Fig. 4h).

Table 3 Temperature and redox estimations calculated with the 2-oxide thermo-oxybarometer (Sauerzapf et al. 2008)

Experimental temperature	Calculated temperature	ΔNNO
955	929	+0.58
940	901	+1.01
910	872	+0.83
880	814	+1.35
850	779	+0.82
750	719	+0.89

Data of Table 1, electronic supplementary item are used for calculations, these are averages of experiments with and without water addition. The accuracy of the 2-oxide thermo-oxybarometer is ±70° for the temperature and ±0.4 log units for the oxygen fugacity (Sauerzapf et al. 2008)

Prehnite breakdown reaction

In the subsolidus experiments, some sparse, complex mineral assemblages with an apparent coronitic structure are locally present (Fig. 6). In the center of these assemblages, a two phase, fine-grained (<1 μm) assemblage has a whole composition that is similar to that of a "dry prehnite". The margins consist of a close intergrowth of plagioclase, which is slightly enriched in An compared to the equilibrium plagioclase, and clinopyroxene. Clinopyroxene is not present elsewhere in the subsolidus experiments, but these ones present in the coronitic assemblages are enriched in CaO and Al_2O_3 compared to the ones of partial melting experiments. According to Liou (1971), prehnite, which is present in our starting material, should react to an assemblage of anorthite + wollastonite when temperature increases (1 prehnite ⇔ 2 anorthite + 1 wollastonite + H_2O). The composition of the assemblage "2 anorthite + 1 wollastonite" corresponds exactly to that of the "dry prehnite", which was analyzed in the corresponding run (Table 1, electronic supplementary item). Since the compositions of the phases forming the close intergrowth network of the rim also deviate slightly from the corresponding equilibrium compositions of plagioclase and clinopyroxene, we interpret the whole coronitic assemblage as a metastable product of the prehnite breakdown reaction. We speculate that the sparse plagioclases with an apparent spongy structure as presented in Fig. 4h, which are much richer in An compared to the equilibrium plagioclases, correspond to metastable relics of such prehnite breakdown reactions. It should be noted that in experimental dehydration melting of mafic systems, relics of An-rich plagioclases may persist metastably for a very long time, even at high water activities (more than 36 days in experiments of Johannes and Koepke 2001).

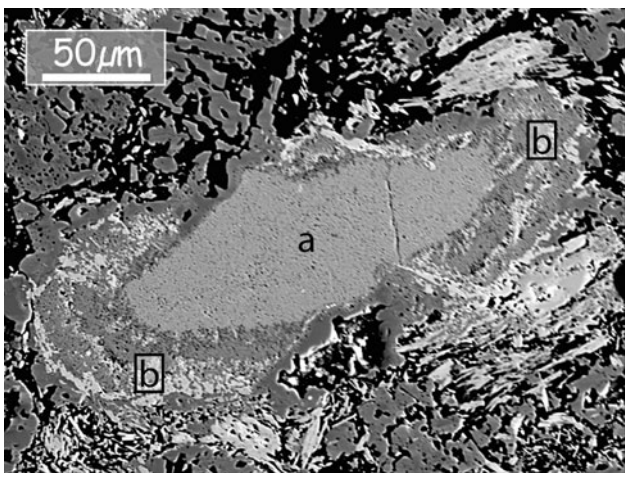

Fig. 6 Backscattered electron image of a coronitic assemblage (750°C with water added experiment) that displays in the center (**a**) a mineral assemblage compositionally similar to "dry prehnite"; it is interpreted as an anorthite + wollastonite assemblage. At the rim (**b**) of this assemblage, an assemblage of metastable plagioclase (Pl_m) and Ca–Al-rich clinopyroxene is observed (brighter). This assemblage is interpreted to be derived from the prehnite breakdown reaction (see the part "Prehnite breakdown reaction" for more details)

Phase compositions in the partial molten system

The phase compositions of the starting material and of the experimental products are listed in Table 1, electronic supplementary item (the main phase composition is listed in Table 4); indicated compositions are averages of mineral compositions in experiments with and without water addition (Fig. 3b). Detailed compositions for each series (with and without water addition) are provided in Table 2, electronic supplementary item. The dependence of olivine composition on temperature is shown in Fig. 7a. The forsterite content (Fo) is nearly identical between the 1,000 and 1,030°C experiments; it may reflect the identical Mg# of the melt in these two runs. The partitioning of Fe and Mg between olivine and melt ($K_{D_{Fe-Mg}}^{Ol-melt} = \frac{X_{Liq}^{Mg}/X_{Ol}^{Mg}}{X_{Liq}^{Fe^{2+}}/X_{Ol}^{Fe^{2+}}}$) is classically considered to be 0.30 ± 0.02 (Roeder and Emslie 1970). Toplis (2005) has reviewed this partitioning coefficient and has proposed a new equation to calculate $K_{D_{Fe-Mg}}^{Ol-melt}$ that can vary as a function of temperature, alkalis, and water. Using this equation for the conditions of our experiments leads to a predicted value of 0.30 ± 0.02. The oxygen fugacity is known in our experiments, the real FeO value (including only the Fe^{2+}) in the melt can be calculated using the Kress and Carmichael (1991) model; the resulting average $K_{D_{Fe-Mg}}^{Ol-melt}$ is 0.28 which is in the accepted range of error according to Toplis (2005), which support the assumption that equilibrium is nearly attained in our experiments.

In the melting experiments, typical clinopyroxene is augite. As expected, its composition varies systematically with temperature. With rising temperature, the wollastonite component and the Mg# increase (from 38 to 44 and from 66 to 78, respectively), as well as the concentration of TiO_2 and Al_2O_3. Clinopyroxene Al_2O_3 content decreases with temperature from 3 to 1.26 wt% (Fig. 7b), whereas the melt Al_2O_3 content is nearly stable. This demonstrates the dependence of the partition coefficient $D_{Al_2O_3}^{Cpx-melt}$ on temperature. It decreases by a factor of ~2 with temperature (from ~0.17 for 1,030°C to ~0.08 for 850°C). Orthopyroxene is enstatite; the wollastonite component and Mg# are, for all temperatures, between 3 and 4 and between 63 and 72, respectively.

In the melting experiments, the anorthite (An) content of plagioclase increases with temperature from 26 to 59. For comparison, in the subsolidus experiments, the An content increases with temperature from 27 to 31.5 (Fig. 7c). In the

Table 4 Composition of the main experimental phases (the complete Table including all experimental phases, analyses standard deviations, and the composition of the starting material minerals are provided in Table 1, electronic supplementary item available from journal website)

Sample	Phase	SiO_2	Al_2O_3	TiO_2	CaO	Na_2O	K_2O	MnO	MgO	FeO	Cr_2O_3	P_2O_5	Total	*N*	Mg#	An%
1,030	melt_recalc.	55.48	17.25	1.54	7.77	5.09	0.20	0.05	3.66	8.94	0.00	0.00	100.00	58	–	–
1,000	melt_recalc.	59.16	17.80	1.29	5.90	5.98	0.27	0.07	2.77	6.76	0.00	0.00	100.00	33	–	–
970	melt_recalc.	62.99	17.81	1.18	4.40	5.85	0.37	0.05	1.99	5.29	0.00	0.09	100.00	38	–	–
955	melt_recalc.	64.36	17.66	1.03	3.83	5.76	0.44	0.04	1.67	4.99	0.02	0.11	100.00	22	–	–
940	melt_recalc.	68.58	17.86	0.88	2.53	4.96	0.83	0.02	0.93	3.16	0.01	0.12	100.00	94	–	–
910	melt_recalc.	69.29	17.35	0.49	2.25	5.46	1.16	0.02	0.65	2.93	0.13	0.06	100.00	27	–	–
880	melt_recalc.	71.19	16.90	0.40	1.88	5.56	1.32	0.02	0.42	2.01	0.06	0.04	100.00	27	–	–
850	melt_recalc.	72.63	16.54	0.29	1.30	4.92	2.21	0.00	0.25	1.62	0.08	0.02	100.00	12	–	–
1,030	Ol	39.21	0.11	0.06	0.32	0.01	0.00	0.14	37.87	22.79	0.00	–	100.54	40	74.76	–
1,000	Ol	38.40	0.17	0.04	0.29	0.04	0.01	0.17	38.68	23.21	–	–	101.01	37	74.80	–
970	Ol	38.44	0.09	0.04	0.30	0.02	0.00	0.21	36.63	24.25	0.00	–	99.98	26	72.91	–
955	Ol	37.39	0.05	0.04	0.25	0.03	0.01	0.22	33.34	27.95	0.02	–	99.34	21	68.01	–
940	Ol	38.64	0.44	0.05	0.46	0.09	0.01	0.23	32.99	27.41	0.00	–	100.34	19	68.21	–
1,030	Cpx	51.92	2.98	0.70	21.37	0.39	0.00	0.08	15.26	7.77	0.01	–	100.50	42	77.77	–
1,000	Cpx	51.18	2.93	0.65	20.90	0.44	0.01	0.11	15.78	8.16	0.03	–	100.17	34	77.52	–
970	Cpx	51.79	2.50	0.60	20.34	0.48	0.01	0.13	15.36	8.53	0.01	–	99.74	30	76.25	–
955	Cpx	51.92	2.17	0.58	19.90	0.48	0.01	0.14	15.07	9.16	0.00	–	99.46	39	74.56	–
940	Cpx	52.76	2.13	0.47	18.83	0.57	0.00	0.16	15.17	10.08	0.01	–	100.20	25	72.87	–
910	Cpx	52.54	1.73	0.41	18.86	0.53	0.02	0.16	14.61	11.11	0.00	–	99.99	47	70.14	–
880	Cpx	52.56	1.47	0.42	18.60	0.56	0.01	0.17	15.52	10.49	0.00	–	99.83	1	72.56	–
850	Cpx	51.42	1.26	0.37	18.22	0.47	0.02	0.16	14.17	13.01	0.00	–	99.13	33	66.08	–
1,000	Pl	52.87	28.92	0.06	12.15	4.59	0.03	0.00	0.12	0.94	–	–	99.69	19	–	59.38
970	Pl	55.34	27.78	0.08	10.54	5.62	0.04	0.00	0.10	0.79	–	–	100.31	27	–	50.92
955	Pl	56.51	27.03	0.05	9.69	5.94	0.04	0.00	0.05	0.59	–	–	99.96	28	–	47.43
940	Pl	58.76	25.88	0.06	8.20	6.97	0.05	0.00	0.06	0.66	–	–	100.66	24	–	39.37
910	Pl	60.98	24.28	0.05	6.46	7.81	0.16	0.00	0.05	0.67	–	–	100.48	26	–	31.41
880	Pl	61.37	23.92	0.06	5.86	7.92	0.17	0.01	0.03	0.55	–	–	99.91	17	–	29.10
850	Pl	61.48	23.76	0.04	5.21	8.35	0.30	0.00	0.02	0.41	–	–	99.62	24	–	25.66
800	Pl	60.02	24.49	0.02	6.35	7.62	0.22	0.01	–	0.35	–	–	99.12	21	–	31.54
750	Pl	60.87	24.00	0.02	5.57	8.22	0.27	0.00	0.02	0.35	–	–	99.35	36	–	27.22

In the sample name column, numbers correspond to the experimental temperature. Compositional values are averages, the detailed compositions of all experiments with and without water addition are provided in Table 2, electronic supplementary item available from journal website. Abbreviations are the same as Table 2 and: Mg# = Mg/(Mg + Fe_{total}) (molar basis), An% = Ca/(Ca + Na + K) (molar basis), *n* number of analyses, *melt_recalc.* melt composition recalculated for a sum = 100%

partly molten system, the FeO_t content of plagioclase increases with temperature, reaching 0.94 wt% in the 1,000°C run. This increase is correlated with increasing FeO_t content in the melt. In contrast, the partition coefficient $D_{FeO_t}^{Pl-melt}$ increases with decreasing temperature. Lundgaard and Tegner (2004) have shown that $D_{FeO_t}^{Pl-melt}$ depends on the redox conditions and on the silica content of the melt ($D_{FeO_t}^{Pl-melt}$ is higher for more oxidizing conditions and for higher silica contents). As our experiments are performed at very similar redox conditions, we attribute this increase of $D_{FeO_t}^{Pl-melt}$ to the increase in silica content of the melt with decreasing temperature.

Titanomagnetite is present from 850 to 1,000°C; it contains between 8 and 14 wt% of TiO_2, while the Al_2O_3 and MgO contents increase with temperature (from 1.55 to 4.21% and from 1.26 to 4.39%, respectively). Ilmenite is present from 850 to 955°C; minor components as SiO_2, Al_2O_3, and MgO globally increase with temperature. The amount of Cr_2O_3 in both oxides is below detection limit.

Amphiboles in the experiments with melt present are edenite and pargasite. As expected, their TiO_2, Al_2O_3, and Na_2O contents increase with temperature. For comparison, they vary from actinolite to hornblende in subsolidus experiments.

Melt is saturated with water in all experiments (presence of bubbles). In the experimental melt obtained with the highest temperature (1,030°C), which displays the largest melt pools, a water content of 4.8 wt% has been determined

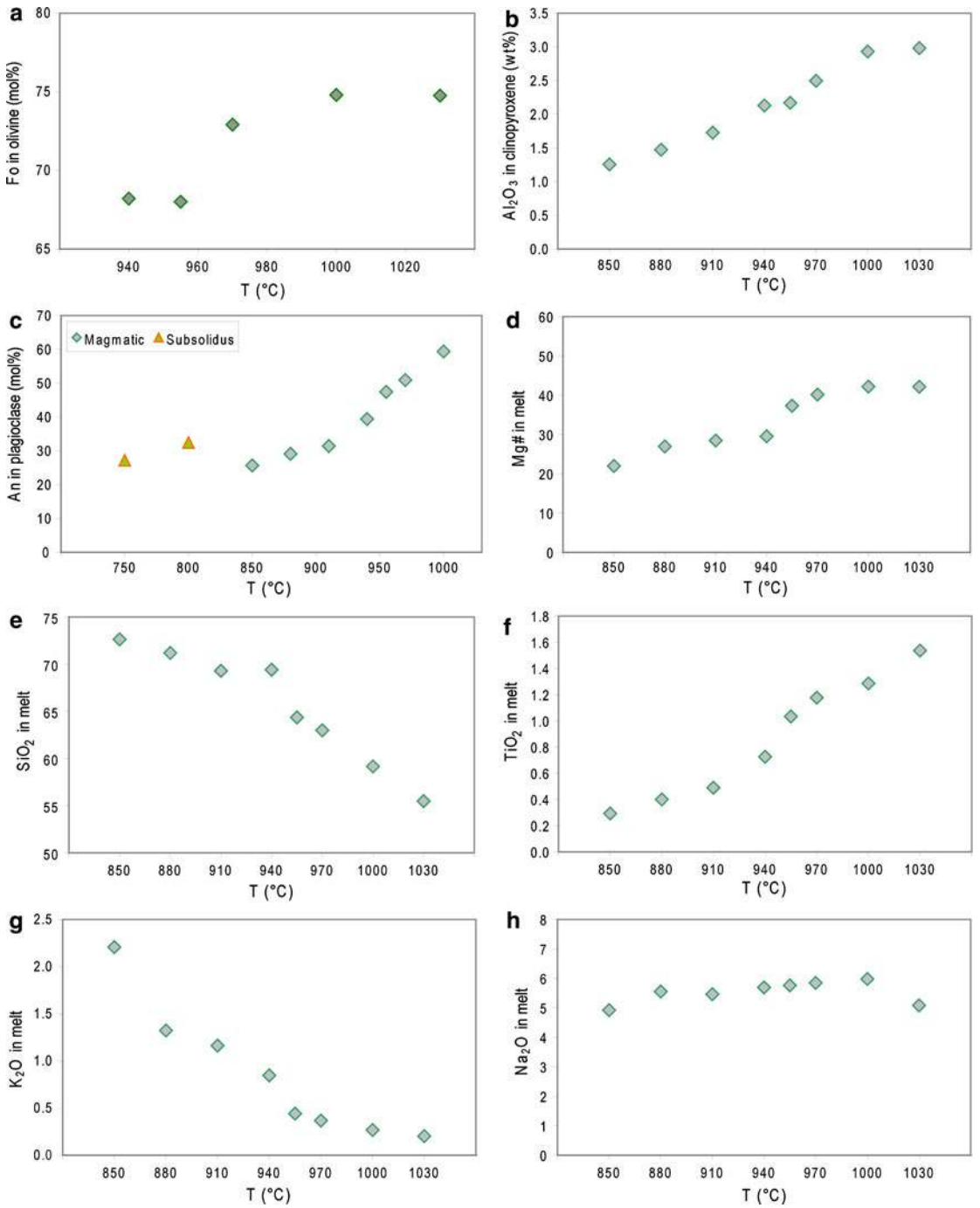

Fig. 7 Compositional features of the experimental phases as a function of temperature. **a** Forsterite content in olivine; **b** Al_2O_3 content of clinopyroxene in the partly molten system; **c** Anorthite content of plagioclase in the partly molten and subsolidus systems; **d** Mg# in melt; **e** SiO_2 in melt; **f** TiO_2 in melt; **g** K_2O in melt; **h** Na_2O in melt

by FTIR (Fourier transformed infrared spectroscopy). The Mg# of the melt increases with temperature from 22 to 42.2 (Fig. 7d). The SiO_2 and K_2O contents decrease with increasing temperature, whereas the TiO_2, MgO, FeO, and CaO contents increase (Fig. 7). Those melts formed at the lowermost temperature (~850°C) reach SiO_2 contents of 72.6 wt%. In a FeO_{total}/MgO versus SiO_2 discriminating diagram (Miyashiro 1974) and in an alkaline ($Na_2O + K_2O$)-FeO_{total}-MgO discriminating diagram (Irvine and Baragar 1971), the experimental melts plot close to the transition between the calc-alkaline and tholeiitic series (Fig. 8).

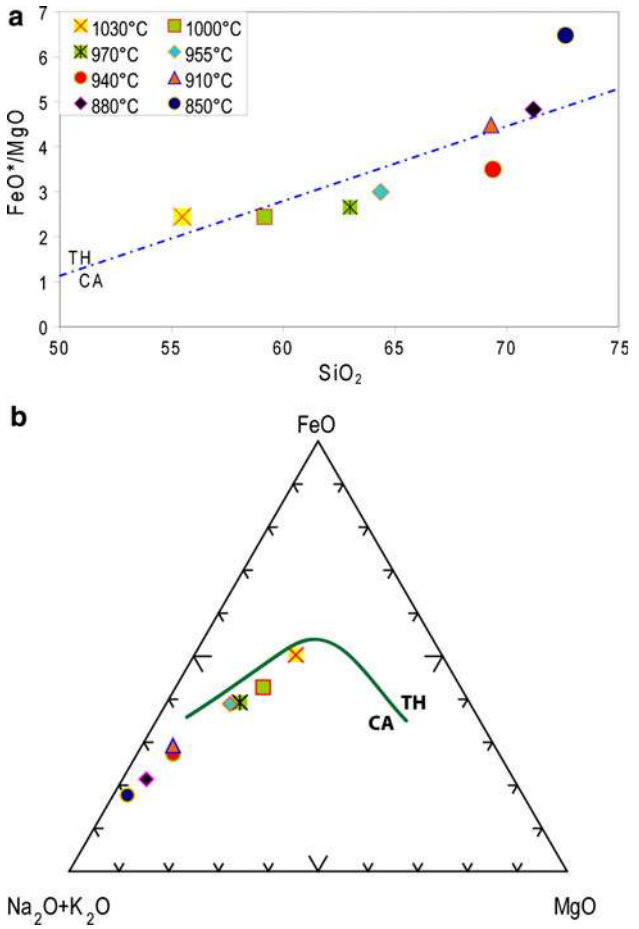

Fig. 8 **a** FeO*/MgO versus SiO_2 diagram from Miyashiro (1974). FeO* FeO_{total}, *TH* tholeiitic field, *CA* calc-alkaline field. **b** Alkaline ($Na_2O + K_2O$)-FeO_{total}-MgO discriminating diagram from Irvine and Baragar (1971)

Discussion

Melt evolution: origin of oceanic plagiogranites at the base of the sheeted dikes

Our experimental melts are compared with other experimental results and with natural data in Fig. 9. For comparison with experimental data from literature, we used MORB fractionation experiments (Dixon-Spulber and Rutherford 1983; Berndt et al. 2005), Fe-Ti MORB fractionation experiments (Juster et al. 1989; Toplis and Carrol 1995), immiscible melt compositions (Dixon and Rutherford 1979), and gabbro, amphibolite and basalt anatexis experiments (Koepke et al. 2004; Beard and Lofgren 1991; and Thy et al. 1999, respectively). Our experiments are relatively similar to those of Beard and Lofgren (1991), and the melt compositions are therefore roughly similar. Nevertheless, our experiments reach lower silica contents despite lower temperature equilibration (850°C in our experiments and 900°C in the Beard and Lofgren ones). The K_2O contents of our experimental melts are similar to most of the Beard and Lofgren (1991) experiments, except for one of their series that display lower contents, and which corresponds to a highly K_2O-depleted starting composition. Melts formed during fractionation experiments using Fe-Ti MORB, and immiscible liquids are depleted in Al_2O_3 and enriched in TiO_2 regarding other experiments. The melt formed in our lower temperature experiments (i.e., with the higher silica content in melt) is slightly depleted in MgO and CaO and slightly enriched in K_2O compared to melts formed during MORB fractionation experiments (Fig. 9). Melts formed during fractionation experiments using MORB compositions display slightly lower K_2O contents than the melts formed during our melting experiments. The K_2O enrichment of our anatectic melts is probably related to the hydrothermal alteration of the starting material. A ternary plot with SiO_2/50-TiO_2-K_2O as apexes can be used to discriminate between immiscibility, fractionation, and anatexis (Fig. 10); indeed only the melts formed during partial melting experiments reach values exceeding 40% for the K_2O apex and below 20% of the TiO_2 apex. Interestingly, in our lower temperature experiments, the composition of the melt is below the line of saturation for TiO_2 in basaltic melts defined by Koepke et al. (2007) (Fig. 9). This allows us to discriminate between gabbro melting (Koepke et al. 2004) and hydrothermally altered dikes melting (Beard and Lofgren 1991, and this study) as only hydrothermally altered dikes melts reach silica contents higher than 68 wt% for TiO_2 concentrations <0.5 wt% (Fig. 9). A combination of TiO_2 versus SiO_2 plot with a ternary plot using SiO_2/50-TiO_2-K_2O as apexes can therefore be used to discriminate on the origin of natural plagiogranites.

To compare our experimental results with natural data, we used published analyses of oceanic plagiogranites interpreted as sheeted dikes partial melts (Gillis and Coogan 2002), as amphibolite partial melts (Gerlach et al. 1981; Pedersen and Malpas 1984; Flagler and Spray 1991), and as differentiated MORB (Beccaluva et al. 1977, 1999; Ghazi et al. 2004). In these studies, the oceanic plagiogranite origin has been inferred from trace element concentrations and structural relationships. As the origin of natural samples is only "inferred", we will not use the comparison with our experimental results to elaborate discriminating tools or diagrams. These natural rocks have relatively homogeneous compositions and globally match our experimental melts. Nevertheless, the melts formed in our lower temperature experiments and oceanic plagiogranites interpreted as differentiated MORB are slightly enriched in K_2O compared to other natural oceanic plagiogranites (Fig. 9). Our experimental melts are also slightly enriched in Al_2O_3 compared to all natural plagiogranites

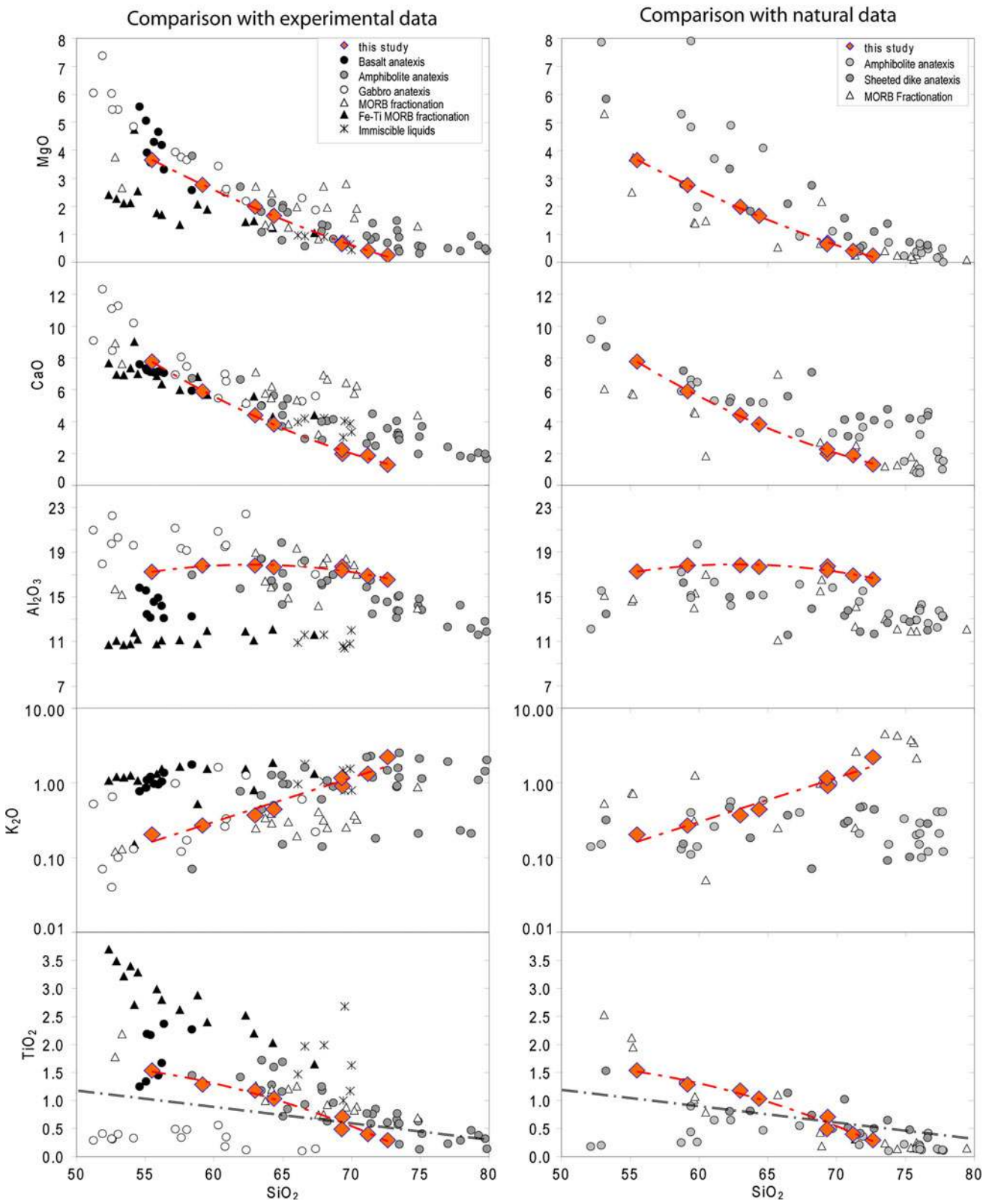

(Fig. 9), it may be attributed to a delay in plagioclase crystallization triggered in our experiments by slightly too oxidizing conditions (e.g., Feig et al. 2006).

To summarize, despite small differences, the melts produced during the experimental hydrous partial melting of hydrothermally altered sheeted dikes have major

◄ **Fig. 9** Harker diagrams (Oxide versus SiO_2). Comparison of melts from this study with other experimental melts (*left column*) and with natural rocks (*right column*). Experimental data are from Dixon-Spulber and Rutherford (1983) and Berndt et al. (2005) for MORB fractionation experiments, from Juster et al. (1989) and Toplis and Carrol (1995) for Fe-Ti MORB fractionation experiments, from Dixon and Rutherford (1979) for immiscible liquid compositions, and from Koepke et al. (2004), Beard and Lofgren (1991), and Thy et al. (1999) for gabbro, amphibolite and basalt anatexis, respectively. Natural data are from Gillis and Coogan (2002) for rocks interpreted as sheeted dikes partial melts, from Gerlach et al. (1981); Pedersen and Malpas (1984) and Flagler and Spray (1991) for rocks interpreted as amphibolite partial melts, and from Beccaluva et al. (1977, 1999) and Ghazi et al. (2004) for rocks interpreted as MORB fractionation. The *dashed line* corresponds to the regression line for the experimental melt compositions of this study. The *dashed-dotted line* in TiO_2 versus SiO_2 diagrams represents the saturation of TiO_2 in basaltic melts defined by Koepke et al. (2007)

element compositions that are relatively similar to other experimental works testing the partial melting of oceanic lithologies and to natural plagiogranites interpreted as products of oceanic lithologies anatexis (Fig. 9). However, the observed major element trends are also relatively similar to those obtained by experiments simulating MORB fractionation and to oceanic plagiogranites interpreted as resulting from MORB fractionation (Fig. 9). A coupled use of TiO_2 versus SiO_2 diagram and ternary SiO_2/50-TiO_2-K_2O diagram can help to discriminate on the plagiogranites origin. Although these diagrams have to be used with care, these are complementary tools for studies which usually use field studies combined with trace element compositions (especially rare earth elements; e.g., Gerlach et al. 1981; Flagler and Spray 1991; Floyd et al. 1998; Luchitskaya et al. 2005; Bonev and Stampfli 2009; Brophy 2008, 2009; Rollinson 2009).

Evolution of the residual minerals: formation of "granoblastic dikes"

At fast spreading ridges, and in ophiolites, the granoblastic dikes that are spatially associated with oceanic plagiogranites present at or close to the base of the sheeted dike complex, and as xenoliths in plagiogranites (Wilson et al. 2006; Koepke et al. 2008; France et al. 2009a), may help to further constrain the plagiogranites origin. If these granoblastic dikes represent the residue after a hydrous partial melting event (Coogan et al. 2003; Gillis 2008; France et al. 2009a), then their mineral compositions should match the ones of our experimental residual minerals.

Detailed petrological descriptions of the granoblastic dike horizon from the Oman ophiolite and from IODP Hole 1256D are given in France et al. (2009a) and Koepke et al. (2008). Gillis (2008) also describe granoblastic dikes (called hornfelsic lithologies) from Pito Deep, Hess Deep, and the Troodos ophiolite. A typical granoblastic assemblage is composed of clinopyroxene, plagioclase, and two oxides (ilmenite and magnetite to titanomagnetite). In IODP Hole 1256D, orthopyroxene is also present. This paragenesis matches well the residual mineral assemblage observed in our partial melting experiments coexisting with a plagiogranitic melt and the paragenesis observed in fractionation experiments using hydrous MORB compositions (Berndt et al. 2005; Feig et al. 2006).

In natural granoblastic dikes, plagioclase compositions range from An_{20} to An_{60}, and clinopyroxene is augite with Mg# varying from 60 to 75. These compositions are similar to our experimental results, in which plagioclases vary from An_{26} to An_{59} (Fig. 7c) and clinopyroxene showing Mg# varying from 66 to 78. Magnetite from granoblastic dikes have lower TiO_2 contents than residual magnetite in our experiments, but as shown by Koepke et al. (2008), they were probably re-equilibrated at lower temperature ($\sim$600°C) during a later, retrograde step ("second" hydrothermal alteration; see Koepke et al. 2008). In contrast, the composition of plagioclase and pyroxene obtained in MORB differentiation experiments (Berndt et al. 2005) does not match the composition of those from granoblastic assemblages. In differentiation experiments, plagioclase compositions range from An_{55} to An_{88}, and clinopyroxene is mostly augites with Mg# varying from 72 to 86.

In our melting experiments, olivine is present at temperatures >940°C; it is absent in the described natural granoblastic dikes. This implies relatively low temperatures associated with their formation.

Gillis (2008), Koepke et al. (2008), and France et al. (2009a) have shown that clinopyroxene from granoblastic dikes are particularly low in Al_2O_3 and TiO_2 (Fig. 11a). France et al. (2009a) show that such compositions are characteristic of granoblastic lithologies (Fig. 11a). Residual clinopyroxene in the present study displays also very low, correlated Al_2O_3 and TiO_2 contents that follow a trend similar to that for granoblastic dike clinopyroxene (Fig. 11b). For comparison, clinopyroxene in MORB differentiation experiments from Berndt et al. (2005) has higher Al_2O_3 contents (between 3.3 and 6.8 wt% instead of 1.2 to 3 wt% in the present study). This difference may be related to the much higher temperature in differentiation experiments. The peculiar TiO_2 versus Al_2O_3 trend obtained for clinopyroxene in the present study seems to be characteristic of hydrous partial melting of previously hydrothermally altered basaltic lithologies and may be linked to the low-temperature conditions coupled to water-saturated conditions at high oxygen fugacities in our experiments. These peculiar conditions prevail in the root zone of the sheeted dike complex. A critical parameter controlling this trend is the oxygen fugacity, which controls the stability of Fe-Ti oxides; the latter in turn controls the Ti budget for Ti partitioning between clinopyroxene and

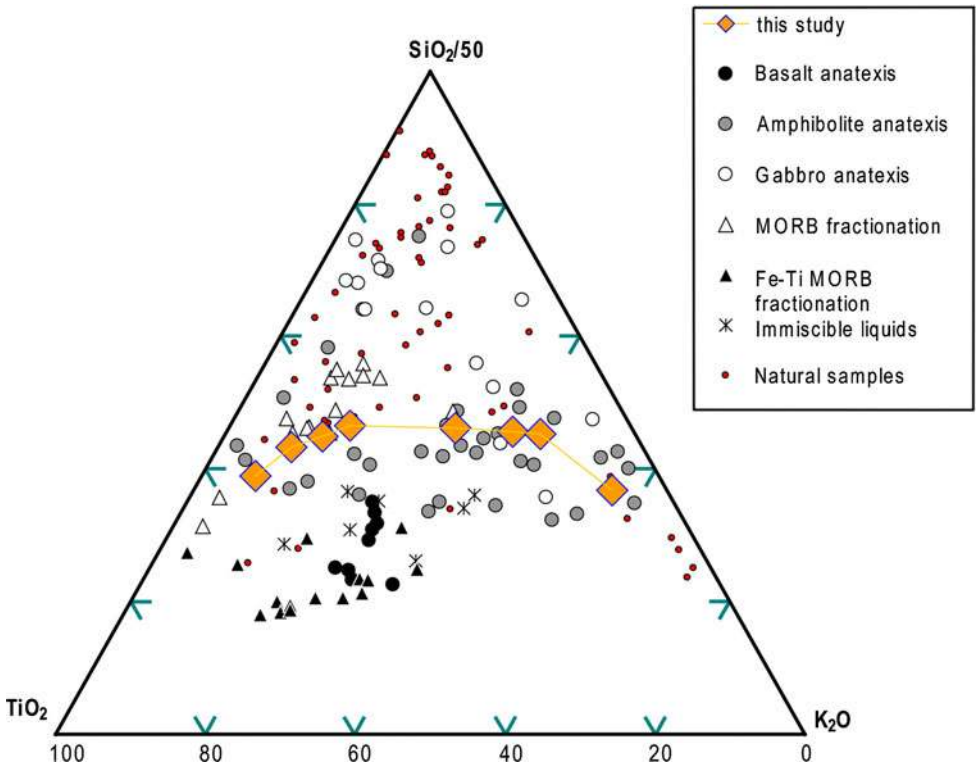

Fig. 10 $SiO_2/50$-TiO_2-K_2O ternary plot comparing melts formed by hydrous partial melting of hydrothermally altered dikes in this study with melts formed by basalt, amphibolite, and gabbro anatexis (Thy et al. 1999; Beard and Lofgren 1991; Koepke et al. 2004, respectively); by fractionation experiments using MORB compositions (Dixon-Spulber and Rutherford 1983; Berndt et al. 2005), and using Fe-Ti MORB compositions (Juster et al. 1989; Toplis and Carrol 1995), and with immiscible melts (Dixon and Rutherford 1979). Natural plagiogranites (natural samples) are also added for comparison (data from: Beccaluva et al. 1977; Gerlach et al. 1981; Pedersen and Malpas 1984; Flagler and Spray 1991; Beccaluva et al. 1999; Gillis and Coogan 2002; Ghazi et al. 2004). Projection is done using a modification of the program of France et al. (2009b), and France and Nicollet (2010)

melt. The experimental trend in the present study has a slightly lower slope than in natural granoblastic dikes; the correspondence between the two trends is best at low TiO_2 and Al_2O_3 contents of clinopyroxene (Fig. 11b). For the strongly oxidizing conditions of our experiments, the stability field of Fe-Ti oxides is larger, and TiO_2 is consequently incorporated in lesser amount into silicates, resulting in a lower TiO_2/Al_2O_3 ratio for clinopyroxene. The observed difference suggests that dehydration and melting reactions at the base of the sheeted dike complex in natural settings proceed at slightly less oxidizing conditions than in our experiments, which were performed at redox conditions corresponding to an oxygen fugacity between QFM+1 and QFM+2. Despite, our new data are the only ones matching the composition of granoblastic dike clinopyroxenes, the lowest TiO_2 and Al_2O_3 values observed in natural samples are not reproduced. Similarly to France et al. (2009a), we propose that these peculiar samples represent reheated samples that have experienced a dehydration stage following a reheating event but without any partial melting.

Figure 11b–c show that TiO_2 and Al_2O_3 contents in clinopyroxene strongly depend on temperature. The relation between Al_2O_3 and temperature can be fitted by a regression curve ($R^2 = 0.98$) with:

$$T = 93.2Al_2O_3 + 742$$

where T is temperature in °C and Al_2O_3 is the Al_2O_3 content in clinopyroxene in wt%. The result can be considered accurate with an uncertainty of ±40°C. This thermometer seems appropriate for estimating equilibration temperatures of the granoblastic dikes and related lithologies at the base of the sheeted dike complex in the oceanic crust. Since pressure and composition also strongly influence the Al_2O_3 content in clinopyroxene, the use of this thermometer is restricted to shallow pressure (100 MPa in this study).

One interesting feature of typical granoblastic dikes is reproduced by our experiments. Granoblastic dikes usually contain clinopyroxenes with countless inclusions of tiny oxide with grain sizes from <1 μm to some tens of μm (Koepke et al. 2008; France et al. 2009a). Manning and

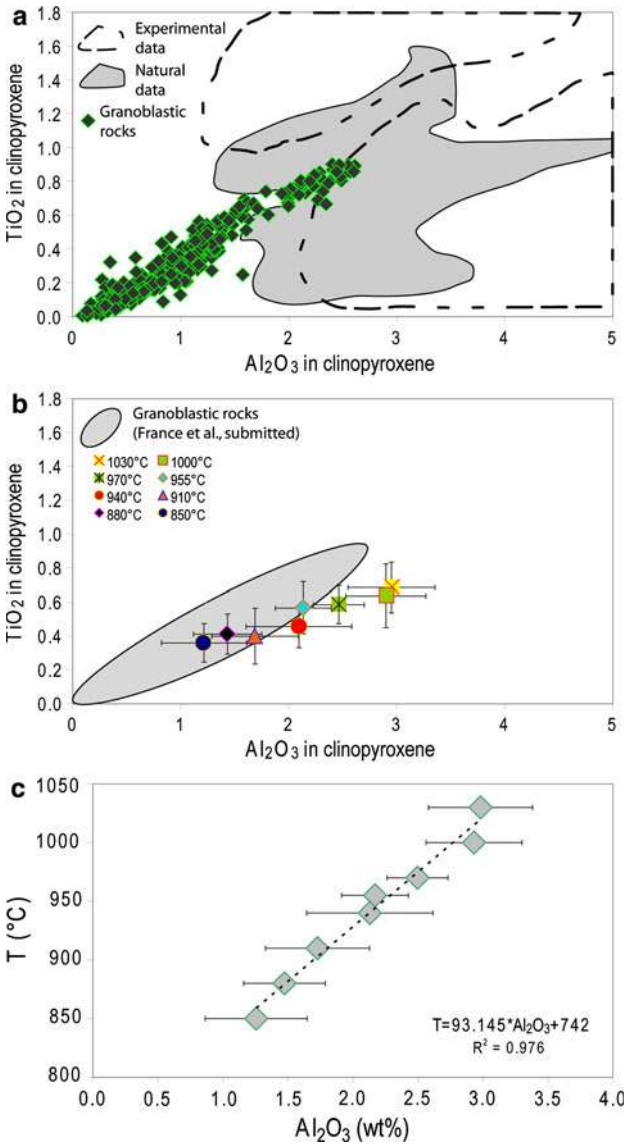

◀ **Fig. 11** Clinopyroxene composition: **a** Correlation between TiO_2 and Al_2O_3. Comparison between clinopyroxenes in granoblastic dikes (*diamonds*; compositions from France et al. 2009a) and experimental and natural data from oceanic crust lithologies; after France et al. (2009a). Experimental data (*dashed field*) are from Snyder et al. (1993), Toplis and Carrol (1995) and Toplis et al. (1994) for Fe-Ti MORB crystallization experiments, from Berndt et al. (2005) and Feig et al. (2006) for hydrous crystallization experiments in primitive MORB-type system, from Grove and Bryan (1983) and Kinzler and Grove (1992) for MORB crystallization experiments, and from Koepke et al. (2004) for clinopyroxenes formed during hydrous partial melting of gabbros. Natural data (*gray field*) for oceanic crust lithologies are from Dziony et al. (2008) for IODP Hole 1256D sheeted dikes not affected by granoblastic imprint, from Miyashita et al. (2003) and Pallister and Hopson (1981) for Oman ophiolite sheeted dikes and gabbros, and from Boudier et al. (2000) and Gerbert-Gaillard (2002) for Oman gabbronorites. **b** Correlation between TiO_2 and Al_2O_3. Comparison between clinopyroxenes of granoblastic rocks (dikes and xenoliths; *gray field*) and clinopyroxenes in the partly molten system of the present study equilibrated at different temperatures. Note that the *gray field* corresponds to the *diamonds* of **a**. **c** Al_2O_3 content (wt%) in clinopyroxene from our experiments as a function of temperature. Standard deviations of analyses are shown. The *dashed line* is the linear regression with the equation $y = 93.145x + 742$ ($R^2 = 0.976$)

MacLeod (1996) have also described metamorphic retrograde clinopyroxenes that are associated with oxides. However, these oxides occur in association with granular clinopyroxene grains at the contact with amphibole, and not as inclusions in clinopyroxenes as in granoblastic dikes. Moreover, these retrograde oxide–clinopyroxene assemblages occur close to late hydrothermal veins in contrast with the ones observed in granoblastic dikes which occur pervasively and associated with fully recrystallized textures. The oxide inclusions present in granoblastic dikes have been ascribed to the prograde evolution of secondary clinopyroxenes developing from complex alteration assemblages originating from primary clinopyroxenes, which include fibrous actinolitic amphibole and extremely fine-grained (<5 μm) coexisting ilmenite and magnetite oxide phases (for details see Koepke et al. 2008; and France et al. 2009a). In our experiments, primary material does not contain clinopyroxene, and new clinopyroxene crystallizes mostly after amphibole. However, we observe similar features, i.e., newly crystallized clinopyroxenes that contain numerous tiny oxide inclusions (Fig. 4g). The presence of these oxide inclusions can be explained by the Mg/Fe budget of the minerals involved in the reaction. Amphibole from the starting material has a lower Mg# (~61) than that of the newly crystallized clinopyroxene (e.g., 78 at 1,000°C). An iron excess is therefore available during clinopyroxene crystallization, resulting in the concentration of iron in the tiny oxides. Since our experiments were performed under highly oxidizing conditions, the stability of Fe-Ti oxides is possible.

The results of our experiments (phase relations, mineral and melt compositions, and other petrographic characteristics such as tiny oxide inclusion in clinopyroxene) support the working models in which granoblastic dikes and associated oceanic plagiogranites at the base of the sheeted dike complex at fast spreading ridges are formed by dehydration and partial melting of previously hydrothermally altered sheeted dikes. Temperatures as high as 1,000°C have been recorded in the granoblastic dikes from several natural settings (Gillis 2008; Koepke et al. 2008; France et al. 2009a); this is clearly above the hydrous solidus temperature determined in this study (~850°C) and implies that hydrous partial melting locally proceeded. Koepke et al. (2008) observed in the granoblastic dikes from IODP Hole 1256D the presence of domains of both "dry" and "hydrous" parageneses. Such "dry" domains, for which significantly higher equilibration temperatures were recorded, probably represent zones which were not, or

less hydrothermally altered, preventing the triggering of hydrous partial melting, since the temperature did not exceed the corresponding dry solidus. These similarities between our experimental results and the corresponding natural settings strongly support an anatectic origin of those plagiogranites that are commonly observed at the base of the sheeted dike complex and that are associated with granoblastic lithologies.

MORB contamination at the base of the sheeted dikes

Our experimental study supports models in which, at fast spreading ridges, the magmatic/hydrothermal interface is a dynamic horizon with magma that can reheat previously hydrothermally altered sheeted dikes during upward migrations of the top of the melt lens (Fig. 12; France et al. 2009a). The absence of olivine in granoblastic dikes of all studied natural settings implies that the temperatures for the partial melting process did not exceed 940°C (Fig. 5), corresponding to a melt fraction $\leq$30%. In our experiments, such melts are highly silicic ($SiO_2 \geq$68.5%; Fig. 7). Hence, they are expected to be highly viscous (for the 850°C experimental melt, and using a theoretical water content of 5 wt%, $\eta = 10^{4.4}$ Pa.s, when calculated using Giordano et al. 2008). Due to the very strong thermal gradient at the interface between the melt lens and the sheeted dikes, melt formation is restricted to a relatively narrow zone at the base of the sheeted dikes, and the amount of such silicic melts is probably relatively low. As the formed melts are of relatively low temperature and highly viscous, they probably do not have the potential to erupt and can therefore get trapped as small intrusive veins near the location of generation (Fig. 12). Such a scenario is described in the core recovered in IODP Hole 1256D; a 20-mm-wide vein of trondhjemitic composition intrudes the granoblastic dikes at 1,404 m below sea-floor (mbsf), ~2 m above the first appearance of gabbro marking the top of the fossil melt lens (Teagle et al. 2006). Felsic igneous rocks are also relatively abundant in the coarse-grained material recovered in junk baskets during hole clearing operations at 1,373 mbsf (Teagle et al. 2006). These leucocratic rock fragments, which consist of plagioclase, quartz, and altered green hornblende, are probably derived from leucocratic intrusions that were not recovered in the core. These felsic lithologies most likely represent products of hydrous partial melting of previously hydrothermally altered sheeted dikes. As hydrous partial melting is believed to occur during upward migrations of the melt lens, the newly formed, highly viscous, silica-rich melt can also be assimilated into the MORB melt within the melt lens (Fig. 12). This melt is transitional between tholeiitic and calc-alkaline (Fig. 8) and represents a source

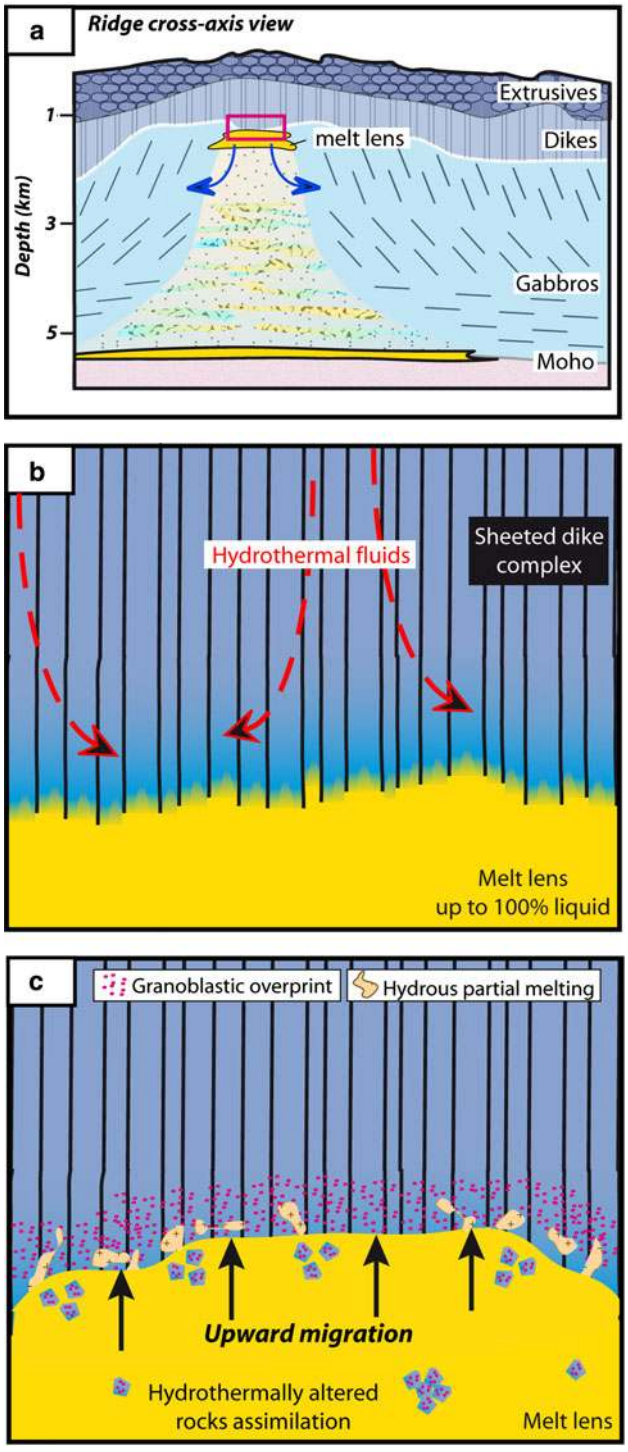

Fig. 12 General schematic model proposed by France et al. (2009a) for the dynamics of the upper melt lens present at fast spreading ridges; **a** Schematic cross-section at the axis of a fast spreading ridge (modified after Sinton and Detrick 1992). The *red rectangle* indicates the location of the *top* of the axial melt lens. **b** Steady state stage with injection of dikes forming the sheeted dike complex. **c** Upward migration of the *top* of the melt lens resulting in reheating, and recrystallization of the base of the dikes (*red dots*) to granoblastic dikes, and in assimilation of xenoliths in the melt lens. Hydrous partial melting of the hydrothermally altered base of the dikes can also occur

of contamination for primary tholeiitic MORB. It will in particular increase the SiO_2 content of the MORB melt, but also the amount of K_2O, rare earth elements and chlorine. This assimilation process may be responsible for the formation of andesitic extrusives which are locally observed in recent oceanic crust (e.g., Haase et al. 2005) and for the chlorine contamination of MORBs (e.g., Michael and Schilling 1989). On the other hand, the residual phases of the hydrous partial melting reaction behave rather refractory, resulting in the occurrence of residual enclaves in the corresponding melts, which display granulite-facies granoblastic parageneses consisting of clinopyroxene + plagioclase + Fe-Ti oxides ± orthopyroxene (Fig. 12). These enclaves are described in IODP Hole 1256D (Teagle et al. 2006; Koepke et al. 2008; France et al. 2009a), at Pito Deep and Hess Deep (Gillis, 2008), and in the Troodos and Oman ophiolites (Gillis 2008; Nicolas et al. 2009; France et al. 2009a). All of these geological settings are portions of present-day or fossil mid-ocean ridges where a dynamic dike/gabbro transition has been proposed.

Conclusion

Partial melting experiments of a sample of the hydrothermally altered sheeted dike complex from the Oman ophiolite have been performed to test the origin of oceanic plagiogranites present at the base of the sheeted dike complex at fast spreading centers. These oceanic plagiogranites are associated with granoblastic lithologies that form the base of the sheeted dike complex and xenoliths in plagiogranites and gabbros. Our experimental results show that:

- Melts produced during partial melting of hydrothermally altered sheeted dikes are highly silicic (up to 72.6 wt%) and match the composition of oceanic plagiogranites.
- The residue of the partial melting experiments matches the modal and peculiar chemical compositions of granoblastic lithologies. Granoblastic lithologies are therefore interpreted to represent the residue after the partial melting event that produces the oceanic plagiogranites.
- The heat source necessary to trigger the partial melting event is believed to be provided by the underlying melt lens. This study therefore supports a model in which the sheeted dike complex/gabbro transition is a dynamic horizon that migrates vertically, with the potential to locally reheat the base of the sheeted dike complex during upward movements.
- Partial melting of hydrothermally altered sheeted dikes and partial assimilation of newly formed melts in the axial melt lens are potential candidates for the contamination (e.g., the chlorine enrichment) observed in some MORB.
- A new thermometer based on the Al content of clinopyroxene is proposed.

Acknowledgments We express our warm thanks to the various people involved at different technical stages of this work: Otto Diedrich for his beautiful thin sections, Wanja Dziony for his assistance with the microprobe analyses, and Tatiana Shishkina for her assistance with the FTIR analyses. Constructive reviews by Etienne Médard, Craig Lundstrom, and an anonymous reviewer are gratefully acknowledged. Dr Salim Al Busaidi, Director General of Minerals, Ministry of Commerce and Industry of the Sultanate of Oman, for allowing us to conduct field work in the Oman ophiolite.

References

Albarède F, Provost A (1977) Petrological and geochemical mass balance equations: an algorithm for least-square fitting and general error analysis. Comput Geosci 3:309–326. doi: 10.1016/0098-3004(77)90007-3

Amri I, Benoit M, Ceuleneer G (1996) Tectonic setting for the genesis of oceanic plagiogranites: evidence from a paleospreading structure in the Oman ophiolite. Earth Planet Sci Lett 139:177–194

Andersen DJ, Lindsley DH, Davidson PM (1993) QUILF: a Pascal program to assess equilibria among Fe-Mg-Mn-Ti oxides, pyroxenes, olivine, and quartz. Comput Geosci 19:1333–1350. doi:10.1016/0098-3004(93)90033-2

Bach W, Erzinger J, Alt JC, Teagle DAH (1996) Chemistry of the lower sheeted dike complex, Hole 504B (Leg 148): influence of magmatic differentiation and hydrothermal alteration. In: Alt JC, Kinoshita H, Stokking LB, Michael PJ (eds) Proceedings of the ODP, Scientific Results, 148, College Station, TX (Ocean Drilling Program), pp 39–55. doi:10.2973/odp.proc.sr.148.114.1996

Ballhaus C, Berry RF, Green DH (1991) High pressure experimental calibration of the olivine—orthopyroxene—spinel oxygen geobarometer: implications for the oxidation state of the upper mantle. Contrib Miner Petrol 107:27–40

Barker F (1979) Trondhjemites, dacites and related rocks. Elsevier, Amsterdam, p 659

Beard JS, Lofgren GE (1989) Effect of water on the composition of partial melts of greenstone and amphibolite. Science 244:195–197

Beard JS, Lofgren GE (1991) Dehydration melting and water saturated melting of basaltic and andesitic greenstones and amphibolites at 1, 3, and 6.9 kb. J Petrol 32:365–401

Beccaluva L, Ohnenstetter D, Ohnenstetter M, Venturelli G (1977) The trace element geochemistry of Corsican ophiolites. Contrib Miner Petrol 64:11–31

Beccaluva L, Chinchilla-Chaves AL, Coltorti M, Giunta G, Siena F, Vaccaro C (1999) Petrological and structural significance of the Santa Elena-Nicoya ophiolitic complex in Costa Rica and geodynamic implications. Eur J Miner 11:1091–1107

Berndt J, Liebske C, Holtz F, Freise M, Nowak M, Ziegenbein D, Hurkuck D, Koepke J (2002) A combined rapid-quench and H2-membrane setup for internally heated pressure vessels: description and application for water solubility in basaltic melts. Am Miner 87:1717–1726

Berndt J, Koepke J, Holtz F (2005) An experimental investigation of the influence of water and oxygen fugacity on differentiation of MORB at 200 MPa. J Petrol 46:135–167

Bonev N, Stampfli G (2009) Gabbro, plagiogranite and associated dykes in the supra-subduction zone Evros Ophiolites, NE Greece. Geol Mag 146(1):72–91. doi:10.1017/S0016756808005396

Boudier F, Godard M, Armbruster C (2000) Significance of gabbronorite occurrence in the crustal section of the Semail ophiolite. Mar Geophys Res 21:307–326. doi:10.1023/A:1026726232402

Brophy JG (2008) A study of rare earth element (REE)-SiO2 variations in felsic liquids generated by basalt fractionation and amphibolite melting: a potential test for discriminating. Contrib Miner Petrol 156:337–357. doi:10.1007/s00410-008-0289-x

Brophy JG (2009) La-SiO_2 and Yb-SiO_2 systematics in mid-ocean ridge magmas: implications for the origin of oceanic plagiogranite. Contrib Miner Petrol 158:99–111. doi:10.1007/s00410-008-0372-3

Coleman RG, Donato MM (1979) Oceanic plagiogranite revisited. In: Barker F (ed) Trondhjemites, dacites, and related rocks. Elsevier, Amsterdam, pp 149–167

Coogan LA (2003) Contaminating the lower crust in the Oman ophiolite. Geology 31(12):1065–1068. doi:10.1130/G20129.1

Coogan LA, Mitchell NC, O'Hara MJ (2003) Roof assimilation at fast spreading ridges: an investigation combining geophysical, geochemical, and field evidence. J Geophys Res 108(B1):2002. doi:10.1029/2001JB001171

Cordier C, Caroff M, Juteau T, Fleutelot C, Hémond C, Drouin M, Cotton J, Bollinger C (2007) Bulk-rock geochemistry and plagioclase zoning in lavas exposed along the northern flank of the Western Blanco depression (Northeast Pacific): insight into open-system magma chamber processes. Lithos 99:289–311

Dixon S, Rutherford MJ (1979) Plagiogranites as late-stage immiscible liquids in ophiolite and mid-oceanic ridge suites: an experimental study. Earth Planet Sci Lett 45:45–60

Dixon-Spulber S, Rutherford MJ (1983) The origin of rhyolite and plagiogranite in oceanic crust: an experimental study. J Petrol 24:1–25

Dubois M (1983) Plagiogranite and hydrothermalism: an approach from Cyprus and Oman ophiolitic complexes. Ph.D. dissertation, University of Nancy 1, France

Dziony W, Koepke J, Holtz F (2008) Data report: petrography and phase analyses in lavas and dikes from the Hole 1256D (ODP Leg 206 and IODP Expedition 309, East Pacific Rise). In: Teagle DAH, Alt JC, Umino S, Miyashita S, Banerjee NR, Wilson DS, and the Expedition 309/312 Scientists. Proceedings of IODP, 309/312, Washington, DC (Integrated Ocean Drilling Program Management International, Inc.). doi:10.2204/iodp.proc.309312.201.2008

Einaudi F, Pezard P, Cocheme JJ, Coulon C, Laverne C, Godard M (2000) Petrography, geochemistry and physical properties of continuous extrusive section from the Sarami Massif, Semail ophiolite. Mar Geophys Res 21:387–407

Ernst WG, Liu J (1998) Experimental phase-equilibrium study of Al- and Ti-contents of calcic amphibole in MORB: a semiquantitative thermobarometer. Am Miner 83:952–969

Feig S, Koepke J, Snow J (2006) Effect of water on tholeiitic basalt phase equilibria—an experimental study under oxidizing conditions. Contrib Miner Petrol 152:611–638. doi: 10.1007/s00410-006-0123-2

Flagler PA, Spray JG (1991) Generation of plagiogranite by amphibolite anatexis in oceanic shear zones. Geology 19:70–73

Floyd PA, Yaliniz MK, Goncuoglu MC (1998) Geochemistry and petrogenesis of intrusive and extrusive ophiolitic plagiogranites, central Anatolian Crystalline Complex, Turkey. Lithos 42:225–241

France L, Nicollet C (2010) MetaRep, an extended CMAS 3D program to visualize mafic (CMAS, ACF-S, ACF-N), and pelitic (AFM-K, AFM-S, AKF-S) projections. Comput Geosci (in press). doi:10.1016/j.cageo.2010.01.001

France L, Ildefonse B, Koepke J (2009a) The sheeted dike/Gabbro transition in the Oman ophiolite and in the IODP Hole 1256D: fossilisation of a dynamic melt lens at fast spreading ridges. Geochem Geophys Geosyst 10:Q10O19. doi:10.1029/2009GC002652

France L, Ouillon N, Chazot G, Kornprobst J, Boivin P (2009b) CMAS 3D, a new program to visualize and project major elements compositions in the CMAS system. Comput Geosci 35:1304–1310. doi:10.1016/j.cageo.2008.07.002

France L, Ildefonse B, Koepke J, Bech F (2010) A new method to estimate the oxidation state of basaltic series from microprobe analyses. J Volcanol Geothermal Res 189:340–346. doi:10.1016/j.jvolgeores.2009.11.023

Gaetani GA, Grove TL, Bryan WB (1993) The influence of water on the petrogenesis of subduction-related igneous rocks. Nature 365:332–334

Gerbert-Gaillard L (2002) Caractérisation géochimique des péridotites de l'ophiolite d'Oman: processus magmatiques aux limites lithosphère-asthénosphère, Ph.D. memoir from Géosciences Montpellier, France, 241 p

Gerlach DC, Leeman WP, Avé Lallemant HG (1981) Petrology and geochemistry of plagiogranite in the Canyon Mountain ophiolite, Oregon. Contrib Miner Petrol 72:82–92

Ghazi AM, Hassanipak AA, Mahoney JJ, Duncan RA (2004) Geochemical characteristics, ^{40}Ar-^{39}Ar ages and original tectonic setting of the Band-e-Zeyarat-Dar Anar ophiolite, Makran accretionary prism, S.E. Iran. Tectonophysics 393:175–196

Gillis KM (2008) The roof of an axial magma chamber: a hornfelsic heat exchanger. Geology 36(4):299–302. doi:10.1130/G24590A.1

Gillis KM, Coogan LA (2002) Anatectic migmatites from the roof of an ocean ridge magma chamber. J Petrol 43:2075–2095

Giordano D, Russell JK, Dingwell DB (2008) Viscosity of magmatic liquids: a model. Earth Planet Sci Lett 271:123–134

Grove TL, Bryan WB (1983) Fractionation of pyroxene-phyric MORB at low pressure: an experimental study. Contrib Miner Petrol 83:293–309. doi:10.1007/BF01160283

Haase KM, Stroncik NA, Hékinian R, Stoffers P (2005) Nb-depleted andesites from the Pacific-Antarctic rise as analogs for early continental crust. Geology 33(12):921–924. doi:10.1130/G21899.1

Hacker BR (1990) Amphibolite-facies to granulite-facies reactions in experimentally deformed, unpowdered amphibolite. Am Miner 75:1349–1361

Hamilton DL, Burnham CW, Osborn EF (1964) The solubility of water and effects of oxygen fugacity and water content on crystallization in mafic magmas. J Petrol 5:21–39

Helz RT (1973) Phase relations of basalt in their melting ranges at $PH_2O = 5$ kb as a function of oxygen fugacity. J Petrol 14:249–302

Holloway JR, Burnham CW (1972) Melting relations of basalt with equilibrium water pressure less than total pressure. J Petrol 13:1–29

Irvine TN, Baragar WRA (1971) A guide to the chemical classification of the common volcanic rocks. Can J Earth Sci 8:532–548

Johannes W, Koepke J (2001) Uncomplete reaction of plagioclase in experimental dehydration melting of amphibolite. Aust J Earth Sci 48:581–590

Juster TC, Grove TL, Perfit MR (1989) Experimental constraints on the generation of FeTi Basalts, Andesites, and Rhyodacites at the Galapagos Spreading Center, 85 W and 95 W. J Geophys Res 94(B7):9251–9274

Juteau T, Bideau D, Dauteuil O, Manac'h G, Naidoo DD, Nehlig P, Ondreas H, Tivey MA, Whipple KX, Delaney JR (1995) A submersible study in the western blanco fracture zone, N.E. Pacific: structure and evolution during the last 1.6 Ma. Mar Geophys Res 17:399–430

Kawamoto T (1996) Experimental constraints on differentiation and H_2O abundance of calc-alkaline magmas. Earth Planet Sci Lett 144:577–589

Kinzler RJ, Grove TL (1992) Primary magmas of mid-ocean ridge basalts 1. Experiments and methods. J Geophys Res 97(B5): 6885–6906. doi:10.1029/91JB02840

Klimm K, Holtz F, Johannes W, King PL (2003) Fractionation of metaluminous A-type granites: an experimental study of the Wangrah Suite, Lachlan Fold Belt, Australia. Precambr Res 124:327–341

Koepke J, Feig ST, Snow J, Freise M (2004) Petrogenesis of oceanic plagiogranites by partial melting of gabbros: an experimental study. Contrib Miner Petrol 146:414–432

Koepke J, Feig ST, Snow J (2005a) Hydrous partial melting within the lower oceanic crust. Terra Nova 17:286–291

Koepke J, Feig ST, Snow J (2005b) Late-stage magmatic evolution of oceanic gabbros as a result of hydrous partial melting: evidence from the ODP Leg 153 drilling at the mid-Atlantic Ridge. Geochem Geophys Geosyst 6:2004GC000805

Koepke J, Berndt J, Feig ST, Holtz F (2007) The formation of SiO_2-rich melts within the deep oceanic crust by hydrous partial melting of gabbros. Contrib Miner Petrol 153:67–84. doi: 10.1007/s00410-006-0135-y

Koepke J, Christie DM, Dziony W, Holtz F, Lattard D, Maclennan J, Park S, Scheibner B, Yamasaki T, Yamazaki S (2008) Petrography of the Dike/Gabbro Transition at IODP Site 1256 (Equatorial Pacific): the evolution of the Granoblastic Dikes. Geochem Geophys Geosyst 9-7:Q07O09. doi:10.1029/2008GC001939

Kress VC, Carmichael ISE (1991) The compressibility of silicate liquids containing Fe_2O_3 and the effect of composition, temperature, oxygen fugacity and pressure on their redox states. Contrib Miner Petrol 108:82–92

Liou JG (1971) Synthesis and stability relations of prehnite, $Ca_2Al_2Si_3O_{10}(OH)_2$. Am Miner 56:507–531

Lippard SJ, Shelton AW, Gass IG (1986) The ophiolite of Northern Oman. In: Geological Society Memoir, 11. Blackwell, Oxford, pp 178

Luchitskaya MV, Morozov OL, Palandzhyan SA (2005) Plagiogranite magmatism in the Mesozoic island-arc structure of the Pekulney Ridge, Chukotka Peninsula, NE Russia. Lithos 79:251–269. doi:10.1016/j.lithos.2004.04.056

Lundgaard KL, Tegner C (2004) Partitioning of ferric and ferrous iron between plagioclase and silicate melt. Contrib Miner Petrol 147:470–483

Malpas J (1979) Two contrasting trondhjemite associations from transported ophiolites in Western Newfoundland: initial report. In: Barker F (ed) Trondhjemites, dacites, and related rocks. Elsevier, Amsterdam, pp 465–487

Manning CE, MacLeod CJ (1996) Fracture-controlled metamorphism of hess deep gabbros, site 894: constraints on the roots of mid-ocean-ridge hydrothermal systems at fast-spreading centers. In: Mével C, Gillis KM, Allan JF, Meyer PS (eds) Proceedings of the Ocean Drilling Program, Scientific Results, vol 147, pp 189–212

Ménot RP (1987) Magmatismes paléozoïques et structuration carbonifère du massif de Belledonne, Alpes françaises. Contraintes nouvelles pour les schémas d'évolution de la chaîne varisque ouest-européenne. Ph.D. dissertation, University Lyon 1, France

Mével C (1988) Metamorphism in ocean layer 3, Gorringe Bank, Eastern Atlantic. Contrib Miner Petrol 100:496–509

Michael PJ, Schilling J-G (1989) Chlorine in mid-ocean ridge magmas: evidence for assimilation of seawater-influenced components. Geochim Cosmochim Acta 53:3131–3143

Miyashiro A (1974) Volcanic rock series in island arcs and active continental margins. Am J Sci 274:321–355

Miyashita S, Adachi Y, Umino S (2003) Along-axis magmatic system in the northern Oman ophiolite: implications of compositional variation of the sheeted dike complex. Geochem Geophys Geosyst 4–9:8617. doi:10.1029/2001GC000235

Nicolas A, Boudier F, Ildefonse B, Ball E (2000) Accretion of Oman and United Arab Emirates ophiolite: discussion of a new structural map. Mar Geophys Res 21:147–179. doi:10.1023/A:1026769727917

Nicolas A, Boudier F, Koepke J, France L, Ildefonse B, Mevel C (2008) Root zone of the sheeted dike complex in the Oman ophiolite. Geochem Geophys Geosyst 9:Q05001. doi:10.1029/2007GC001918

Nicolas A, Boudier F, France L (2009) Subsidence in magma chamber and the development of magmatic foliation in Oman ophiolite gabbros. Earth Planet Sci Lett 284:76–87. doi:10.1016/j.epsl.2009.04.012

Niu Y, Gilmore T, Mackie S, Greig A, Bach W (2002) Mineral chemistry, whole-rock compositions, and petrogenesis of Leg 176 gabbros: data and discussion. In: Natland JH, Dick HJB, Miller DJ, Von Herzen RP (eds) Proceedings of ODP, Scientific Results 176. Ocean Drilling Program, College Station, TX, pp 1–60, [Online] http://www-odp.tamu.edu/publications/176_SR/VOLUME/CHAPTERS/SR176_08.PDF. (Cited Aug 23, 2003)

Pallister JS, Hopson CA (1981) Samail Ophiolite Plutonic Suite: field relations, phase variation, cryptic variation and layering, and a model of a spreading ridge magma chamber. J Geophys Res 86(B4):2593–2644

Pallister JS, Knight RJ (1981) Rare-earth element geochemistry of the Samail Ophiolite near Ibra, Oman. J Geophys Res 86(B4):2673–2697

Patino Douce AE, Beard JS (1995) Dehydration-melting of biotite gneiss and quartz amphibolite from 3 to 15 kbar. J Petrol 36:707–738

Pedersen RB, Malpas J (1984) The origin of oceanic plagiogranites from the Karmoy ophiolite, Western Norway. Contrib Miner Petrol 88:36–52

Philpotts AR (1982) Compositions of immiscible liquids in volcanic rocks. Contrib Miner Petrol 80:201–218

Pollock ME, Klein EM, Karson JA, Coleman DS (2009) Compositions of dikes and lavas from the Pito Deep Rift: implications for crustal accretion at superfast spreading centers. J Geophys Res 114:B03207. doi:10.1029/2007JB005436

Pouchou JL, Pichoir F (1991) Quantitative analysis of homogeneous or stratified microvolumes applying the model ''PAP''. In: Heinrich KFJ, Newbury DE (eds) Electron probe quantification. Plenum Press, New York, pp 31–75

Prouteau G, Scaillet B, Pichavant M, Maury RC (1999) Fluid-present melting of ocean crust in subduction zones. Geology 27(12): 1111–1114

Rao DR, Rai H, Kumar JS (2004) Origin of oceanic plagiogranite in the Nidar ophiolitic sequence of eastern Ladakh, India. Curr Sci 87(7):999–1005

Rapp RP, Watson EB (1995) Dehydration melting of metabasalt at 8–32 kbar: implications for continental growth and crustmantle recycling. J Petrol 36:891–931

Rapp RP, Watson EB, Miller CF (1991) Partial melting of amphibolite/eclogite and the origin of Archean trondhjemites and tonalites. Precambr Res 51:1–25

Rochette P, Jenatton L, Dupuy C, Boudier F, Reuber I (1991) Diabase dikes emplacement in the Oman ophiolite: a magnetic fabric study with reference to geochemistry. In: Peters T, Nicolas A, Coleman RG (eds) Ophiolite genesis and evolution of the oceanic lithosphere. Kluwer, Dordrecht, pp 39–54

Roeder PL, Emslie RF (1970) Olivine–liquid equilibrium. Contrib Miner Petrol 29:275–289

Rollinson H (2009) New models for the genesis of plagiogranites in the Oman Ophiolite. Lithos 112:603–614. doi: 10.1016/j.lithos.2009.06.006

Ross K, Elthon D (1993) Cumulates for strongly depleted mid-ocean-ridge basalt. Nature 365(6449):826–829

Rushmer T (1991) Partial melting of two amphibolites: contrasting experimental results under fluid-absent conditions. Contrib Miner Petrol 107:41–59

Rushmer T (1993) Experimental high-pressure granulites: some applications to natural mafic xenolith suites and Archean granulite terranes. Geology 21:411–414

Sato H (1978) Segregation vesicles and immiscible liquid droplets in ocean-floor basalt of Hole 396B, IPOD/DSDP Leg 46. In: Dimitriev L, Heirtzler J et al (eds) Initial reports of the deep sea drilling project, vol 46. U.S. Government Printing Office, Washington, pp 283–291

Sauerzapf U, Lattard D, Burchard M, Engelmann R (2008) The titanomagnetite-ilmenite equilibrium: new experimental data and thermo-oxybarometric application to the crystallization of basic to intermediate rocks. J Petrol 49(6):1161–1185. doi: 10.1093/petrology/egn021

Scaillet B, Pichavant M, Roux J, Humbert G, Lefèvre A (1992) Improvements of the Shaw membrane technique for measurement and control of fH2 at high temperatures and pressures. Am Miner 77:647–655

Selbekk RS, Furnes H, Pedersen RB, Skjerlie KP (1998) Contrasting tonalite genesis in the Lyngen magmatic complex, north Norwegian Caledonides. Lithos 42:243–268

Sen C, Dunn T (1994) Dehydration melting of a basaltic composition amphibolite at 1.5 and 2.0 GPa: implications for the origin of adakites. Contrib Miner Petrol 117:394–409

Shastry A, Srivastava RK, Chandra R, Jenner GA (2001) Fe-Ti enriched mafic rocks from South Andaman ophioite suite: implications of late stage liquid immiscibility. Curr Sci 80:453–454

Sinton JM, Detrick RS (1992) Mid-ocean ridge magma chambers. J Geophys Res 97:197–216. doi:10.1029/91JB02508

Snyder D, Carmichael ISE, Wiebe RA (1993) Experimental study of liquid evolution in an Fe-rich, layered mafic intrusion: constraints of Fe-Ti oxide precipitation on the T-fO_2 and T-ρ paths of tholeiitic magmas. Contrib Miner Petrol 113:73–86. doi: 10.1007/BF00320832

Spray JG, Dunning GR (1991) A U/Pb age for the Shetland Islands oceanic fragment, Scottish Caledonides: evidence from anatectic plagiogranites in 'layer 3' shear zones. Geol Mag 128:667–671

Stakes DS, Taylor HP (2003) Magmatic, metamorphic and tectonic processes in ophiolite genesis: oxygen isotope and chemical studies on the origin of large plagiogranite bodies in northern Oman, and their relationship to the overlying massive sulphide deposits. Geol Soc Lond Spec Publ 218:315–351. doi:10.1144/GSL.SP.2003.218.01.17

Teagle DAH, Alt JC, Umino S, Miyashita S, Banerjee NR, Wilson DS, and the Expedition 309/312 Scientists (2006) Superfast spreading rate crust 2 and 3. Proceedings of Integrated Ocean Drill Program 309/312. doi:10.2204/iodp.proc.309312.2006

Thy P, Lesher CE, Mayfield JD (1999) Low-pressure melting studies of basalt and basaltic andesite from the southeast Greenland continental margin and the origin of dacites at site 917. In: Larsen HC, Duncan RA, Allan JF, Brooks K (eds) Proceedings of the ODP, science research, vol 163. Ocean Drilling Program, College Station, pp 95–112

Toplis MJ (2005) The thermodynamics of iron and magnesium partitioning between olivine and liquid: criteria for assessing and predicting equilibrium in natural and experimental systems. Contrib Miner Petrol 149:22–39

Toplis MJ, Carrol MR (1995) An experimental study of the influence of oxygen fugacity on Fe-Ti oxide stability, phase relations, and mineral–melt equilibria in ferro-basaltic systems. J Petrol 36–5:1137–1170

Toplis MJ, Libourel G, Carroll MR (1994) The role of phosphorus in crystallisation processes of basalt: an experimental study. Geochim Cosmochim Acta 58(2):797–810. doi:10.1016/0016-7037(94)90506-1

Twinning K (1996) Origin of plagiogranites in the Troodos ophiolite, Cyprus. The Ninth Keck Research Symposium in Geology, pp 245–248

Ulrich T, Borsien G-R (1996) Fedoz metagabbros and Forno metabasalt (Val Malenco, N Italy): comparative petrographic and geochemical investigations. Schweiz Miner Petrogr Mitt 76:521–535

Umino S, Miyashita S, Hotta F, Adachi Y (2003) Along-strike variation of the sheeted dike complex in the Oman Ophiolite: insights into subaxial ridge segment structures and the magma plumbing system. Geochem Geophys Geosyst 4–9:8618. doi: 10.1029/2001GC000233

Veksler IV, Dorfman AM, Borisov AA, Wirth R, Dingwell DB (2007) Liquid immiscibility and the evolution of basaltic magma. J Petrol 48(11):2187–2210. doi:10.1093/petrology/emg056

Wilson DS et al (2006) Drilling to gabbro in intact ocean crust. Science 312:1016–1020

Wolf MB, Wyllie PJ (1994) Dehydration-melting of amphibolite at 10 kbar: the effects of temperature and time. Contrib Miner Petrol 115:369–383